AD-A140 711 ANALYSIS OF TRANSMISSION LINES ON SEMICONDUCTOR SUBSTRATE(U) TEXAS UNIV AT AUSTIN DEPT OF ELECTRICAL ENGINEERING Y C SHIH ET AL. 01 MAR 84 UT-MW-84-2 1/1

UNCLASSIFIED N00014-79-C-0553 F/G 9/5 NL

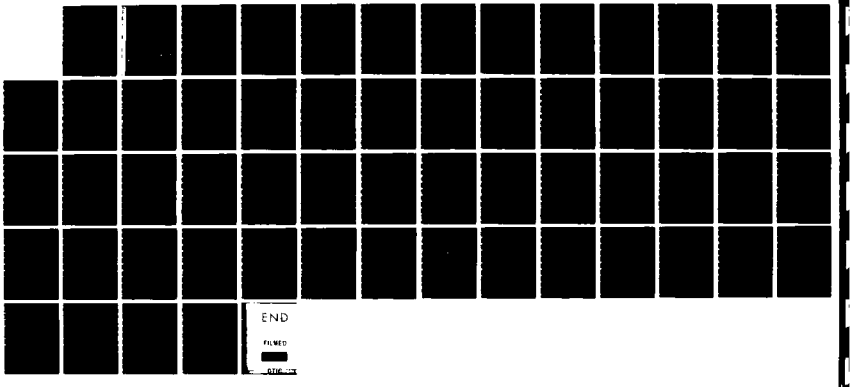

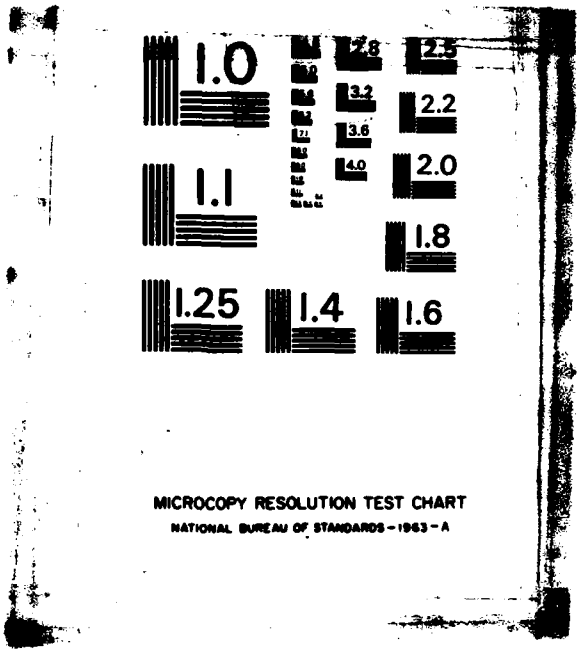
1.0
1.1
1.25
1.4
1.6
1.8
2.0
2.2
2.5
3.2
3.6
4.0
MICROCOPY RESOLUTION TEST CHART
NATIONAL BUREAU OF STANDARDS - 1963 - A

MICROWAVE LABORATORY REPORT No. 84-2

ANALYSIS OF TRANSMISSION LINES ON SEMICONDUCTOR SUBSTRATE

TECHNICAL REPORT

YI-CHI SHIH AND TATSUO ITOH

MARCH 1, 1984

OFFICE OF NAVAL RESEARCH

CONTRACT NO. N00014-79-C-0553

UNIVERSITY OF TEXAS

DEPARTMENT OF ELECTRICAL ENIGNEERING

AUSTIN, TX 78712

APPROVED FOR PUBLIC RELEASE

DISTRIBUTION UNLIMITED

Unclassified

SECURITY CLASSIFICATION OF THIS PAGE (When Data Entered)

REPORT DOCUMENTATION PAGE		READ INSTRUCTIONS BEFORE COMPLETING FORM
1. REPORT NUMBER MW No. 84-2	2. GOVT ACCESSION NO. A140 711	3. RECIPIENT'S CATALOG NUMBER
4. TITLE (and Subtitle) Analysis of Transmission lines on semiconductor Substrate		5. TYPE OF REPORT & PERIOD COVERED Technical Report 6. PERFORMING ORG. REPORT NUMBER
7. AUTHOR(s) Yi-Chi Shih and Tatsuo Itoh		8. CONTRACT OR GRANT NUMBER(s) N00014-79-C-0553
9. PERFORMING ORGANIZATION NAME AND ADDRESS University of Texas at Austin Department of Electrical Engineering Austin, Texas 78712		10. PROGRAM ELEMENT, PROJECT, TASK AREA & WORK UNIT NUMBERS
11. CONTROLLING OFFICE NAME AND ADDRESS Office of Naval Research Arlington, VA 22217		12. REPORT DATE March 1, 1984 13. NUMBER OF PAGES
14. MONITORING AGENCY NAME & ADDRESS(if different from Controlling Office)		15. SECURITY CLASS. (of this report) Unclassified 15a. DECLASSIFICATION/DOWNGRADING SCHEDULE

16. DISTRIBUTION STATEMENT (of this Report)

Unlimited

17. DISTRIBUTION STATEMENT (of the abstract entered in Block 20, if different from Report)

N/A

18. SUPPLEMENTARY NOTES

19. KEY WORDS (Continue on reverse side if necessary and identify by block number)

Microstrip line, Coplanar waveguide, Conductor-backed coplanar waveguide, slow-wave factor, MIS, Schottky barrier.

20. ABSTRACT (Continue on reverse side if necessary and identify by block number)

An efficient numerical method based on the application of Galerkin's method in the spectral domain is proposed to obtain the propagation constant and characteristic impedance of planar transmission lines used in monolithic microwave integrated circuits. First, the transmission-line properties of a conductor-backed coplanar waveguide are analyzed. For a fixed substrate thickness, the characteristic impedance and phase constant may —

DD FORM 1 JAN 73 1473 EDITION OF 1 NOV 65 IS OBSOLETE S/N 0102-014-6601

Unclassified

SECURITY CLASSIFICATION OF THIS PAGE (When Data Entered)

MICROWAVE LABORATORY REPORT No. 84-2

ANALYSIS OF TRANSMISSION LINES ON SEMICONDUCTOR SUBSTRATE

TECHNICAL REPORT

YI-CHI SHIH AND TATSUO ITOH

MARCH 1, 1984

OFFICE OF NAVAL RESEARCH

CONTRACT NO. N00014-79-C-0553

UNIVERSITY OF TEXAS

DEPARTMENT OF ELECTRICAL ENIGNEERING

AUSTIN, TX 78712

ANALYSIS OF TRANSMISSION LINES ON SEMICONDUCTOR SUBSTRATE

ABSTRACT

An efficient numerical method based on the application of Galerkin's method in the spectral domain is proposed to obtain the propagation constant and characteristic impedance of planar transmission lines used in monolithic microwave integrated circuits. First, the transmission-line properties of a conductor-backed coplanar waveguide are analyzed. For a fixed substrate thickness, the characteristic impedance and phase constant may be varied independently by adjusting the width of the center strip and slots in the transmission line. Then microstrip lines and coplanar waveguides formed with MIS and Schottky barrier contacts are analyzed. Depending on the frequency and the resistivity of the semiconductor substrate, three different types of fundamental modes are predicted. The calculated slow-wave factors and attenuation constants agree well with experimental results.

TABLE OF CONTENTS

LIST OF TABLES

LIST OF FIGURES

I. INTRODUCTION

Monolithic microwave integrated circuits (MMIC) based on gallium arsenide (GaAs) technologies are being considered seriously as viable candidates for satellite communication systems, airborn radar systems, and other applications [1-4]. The low-loss properties of semi-insulating GaAs, combined with the excellent microwave performance of metal-semiconductor field-effect transistors (MESFET's) [5], make it possible to design truly monolithic microwave integrated circuits. By monolithic we mean an approach wherein all passive and active circuit elements and interconnections are formed on the substrate by some deposition scheme, such as epitaxy, ion implantation, sputtering, and evaporation.

The monolithic approach makes it possible to fabricate circuits of small size and light weight, and this approach eliminates wire bonding between components in the circuits. Small size allows batch processing of hundreds of circuits per wafer. The use of batch processing and the elimination of wire bonding lowers the cost of manufacture and improves the reliability, reproducibility, and operating bandwidth.

However, as the physical dimensions of the circuit components become smaller, it becomes more difficult to trim and trouble-shoot a working circuit. To minimize the need for trimming and to simplify trouble-shooting, a computer-aided design (CAD) technique is essential. Another potential problem that arises due

to the small chip size is undesired RF coupling within the circuit. To avoid the coupling problem and to create an efficient CAD program requires a thorough knowledge of the transmission properties of planar transmission lines formed on semiconductor substrates.

On a planar substrate, there are basically four types of transmission lines available, as shown in Fig. 1. They are microstrip line (Fig. 1(a)), slot line (Fig. 1(b)), coplanar waveguide (Fig. 1(c), and coplanar strips (Fig. 1(d)). In the past two decades, these transmission lines have been studied fruitfully using various analytical and numerical techniques such as conformal mapping [6,7], finite difference [8], finite element [9], integral equation [10], spectral domain [11,12,13], and many other methods [14,15,16]. Based on the considerations of chip yield and electrical performance, microstrip lines and coplanar waveguides are considered to be the most suitable for MMICs [17].

One way of keeping material costs down is to make the substrate as thin as possible. Since thin GaAs substrate is fragile, a bottom-side ground plate is used to increase the mechanical strength of the coplanar waveguide circuits. This requirement results in a conductor-backed coplanar waveguide as shown in Fig. 2. Because of the thin substrate, the electrical effect of the additional conductor plane backing is important. Since no analytical results have been reported on the propagation characteristics of such a structure, this is the first subject to be studied.

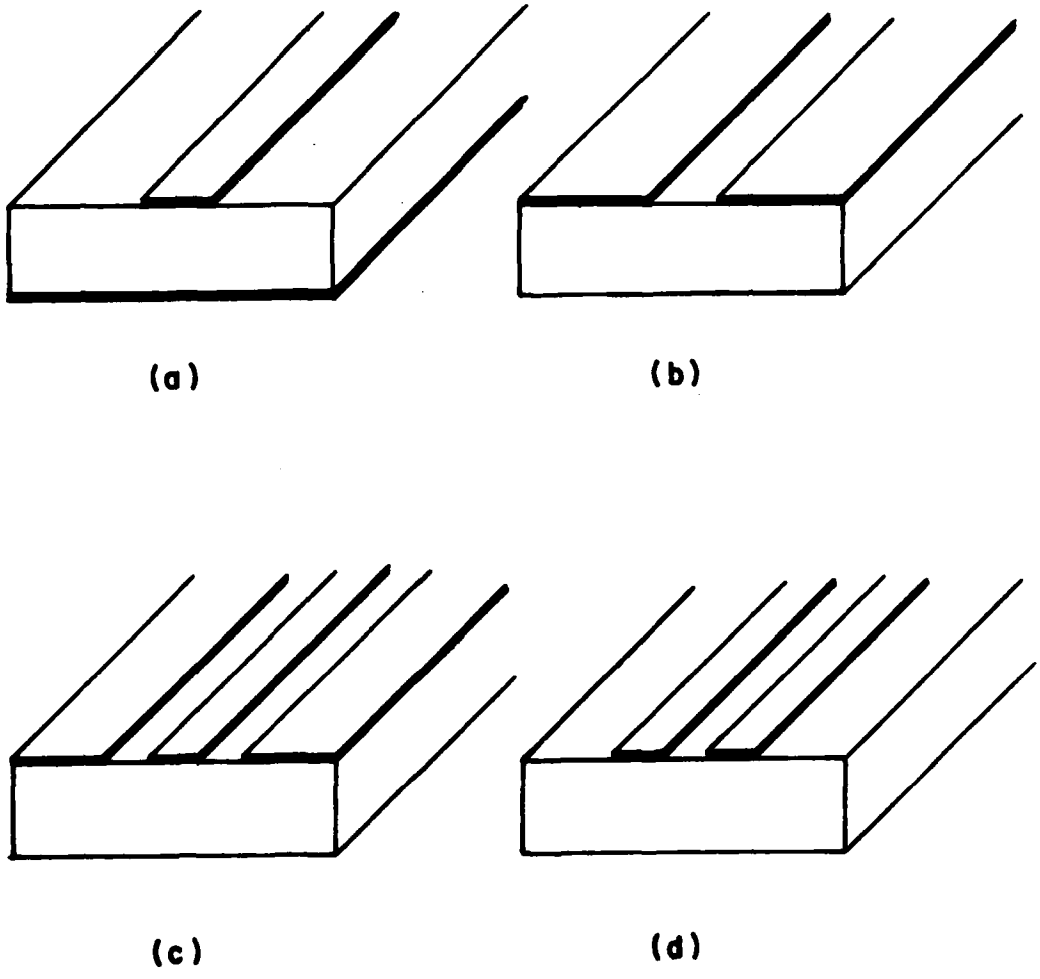

Fig. 1. Transmission lines in MMICs. (a) Microstrip, (b) Slotline, (c) Coplanar waveguide, (d) Coplanar strips.

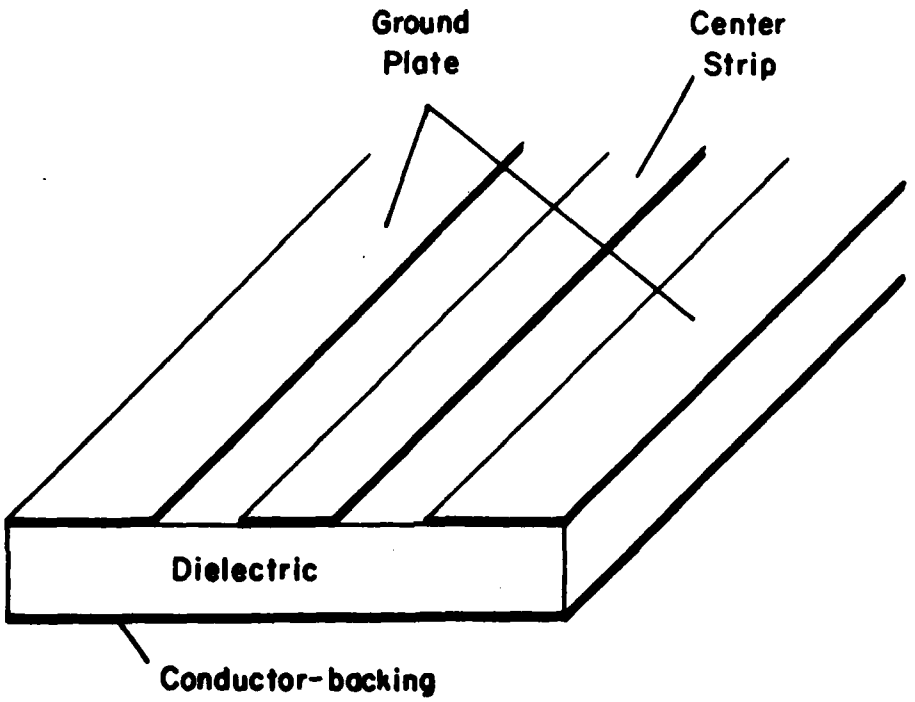

Fig. 2. Geometry of conductor-backed coplanar waveguide.

Other structures to be studied include slow-wave transmission lines formed with metal-insulator-semiconducto contacts shown in Fig. 3. The existence of the slow-wav has been experimentally observed on MIS and Schottky-barrie strip lines [18,19] as well as coplanar waveguides [20]. B of the reduction in dimensions of the distributed passive c these slow-wave transmission lines could be advantageous in design of MMICs. Some applications employing these structu been proposed in the design of filters, directional coupler and phase shifters [22].

In the following chapters, the conductor-backed c waveguide and the slow-wave transmission lines mentioned ab be analyzed using a full wave analysis in the spectral doma Transmission line characteristics such as propagation const characteristic impedances will be calculated and compared w available measurements.

II. FORMULATION

The spectral domain technique was developed a few ago for efficient numerical analysis of printed transmissio [11,12,13,23]. Unlike quasi-static approximations, this me a full wave analysis which can predict the frequency-depend properties required in broadband design. It is superior to numerical methods because of the efficiency of numerical ca and the ease of formulation [24].

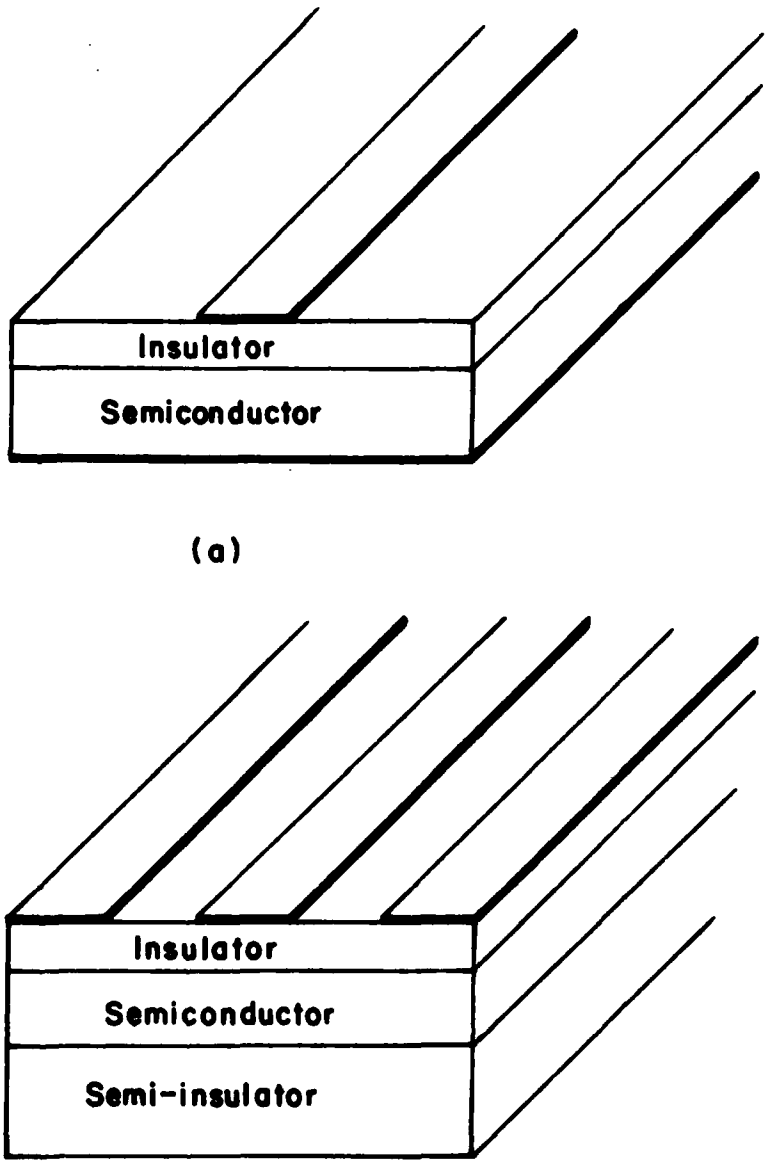

Fig. 3. MIS slow-wave structures. (a) MIS microstrip line, (b) MIS coplanar waveguide.

A. Propagation Constant

The cross-sectional view of a conductor-backed coplanar waveguide is given in Fig. 4. The coordinate system is defined in a manner such that wave propagations take place in the z-direction. The area of the cross-section is divided into two regions by the boundary at y = d with each region containing homogeneous dielectric material.

In conventional space domain analysis [25], this structure may be analyzed by first formulating the following coupled homogeneous integral equations and then solving for the unknown propagation constant:

$$\int [Y_{zz}(x - x',\beta)E_z(x') + Y_{zx}(x - x',\beta)E_x(x')]\, dx' = J_z(x) \qquad (1a)$$

$$\int [Y_{xz}(x - x',\beta)E_z(x') + Y_{xx}(x - x',\beta)E_x(x')]\, dx' = J_x(x) \qquad (1b)$$

where E_x, E_z, J_x and J_z are unknown electric field and current components on the boundary y = d and the Green's functions (admittance functions) Y_{zz}, etc., are functions of the propagation constant β. The boundary conditions at y = d require that E_x and E_z be zero except on the slots where J_x and J_z are required to be zero. Therefore, these equations may be solved provided that Y_{zz}, etc., are given. However, for the inhomogeneous structures, the Green's functions are not available in closed forms.

In the spectral domain formulation, the convolutional type of coupled integral equations (1a,b) are Fourier

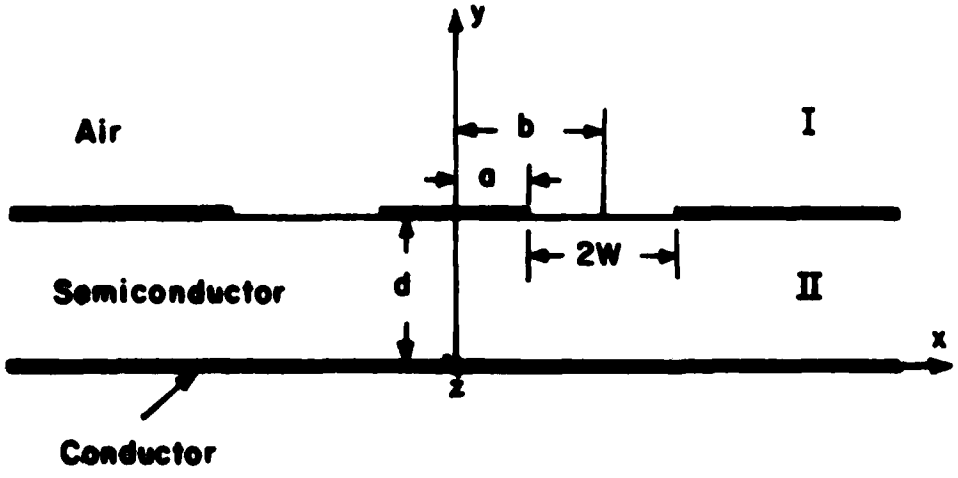

Fig. 4. Cross-sectional view of conductor-backed coplanar waveguide.

transformed to yield the algebraic equations:

$$\tilde{Y}_{zz}(\alpha,\beta)\tilde{E}_z(\alpha) + \tilde{Y}_{zx}(\alpha,\beta)\tilde{E}_x(\alpha) = \tilde{J}_z(\alpha) \qquad (2a)$$

$$\tilde{Y}_{xz}(\alpha,\beta)\tilde{E}_z(\alpha) + \tilde{Y}_{xx}(\alpha,\beta)\tilde{E}_x(\alpha) = \tilde{J}_x(\alpha) \qquad (2b)$$

where the quantities with a tilde ($\sim$) are Fourier transforms of the corresponding quantities. The Fourier transform is defined as

$$\tilde{\phi}(\alpha) = \frac{1}{\sqrt{2\pi}} \int_{-\infty}^{\infty} \phi(x) e^{j\alpha x}\, dx \qquad (3)$$

In addition to β, the algebraic equations (2a,b) contain four other unknowns $\tilde{J}_z$, $\tilde{J}_x$, $\tilde{E}_z$ and $\tilde{E}_x$.

The Green's admittance functions are derived as follows. First, the hybrid fields are expressed in terms of superposition of TM-to-y and TE-to-y expressions by way of vector potentials. The electric and magnetic vector potentials are defined in both regions (i = 1,2) as

$$\vec{\phi}^h_i(x,yz,) = \vec{a}_y\, \phi^h_{yi}(x,y)\, e^{-j\beta z} \quad , \quad i = 1,2 \qquad (4a)$$

$$\vec{\phi}^e_i(x,y,z) = \vec{a}_y\, \phi^e_{yi}(x,y)\, e^{-j\beta z} \quad , \quad i = 1,2 \qquad (4b)$$

where the time convention $e^{j\omega t}$ is implied, and harmonic solutions in the z direction are assumed. Beta (β) is the phase constant and $\vec{a}_y$ denotes the unit vector in the y direction. Since the vector potentials satisfy the vector Helmholtz equation, the scalar functions ϕ^h_{yi} and ϕ^e_{yi} should satisfy the scalar Helmholtz equation

$$\frac{\partial^2 \phi^h_{yi}}{\partial x^2} + \frac{\partial^2 \phi^h_{yi}}{2y^2} + (\varepsilon_{ri} k_o^2 - \beta^2)\phi^h_{yi} = 0 \qquad (5a)$$

$$\frac{\partial^2 \phi^e_{yi}}{\partial x^2} + \frac{\partial^2 \phi^e_{yi}}{\partial y^2} + (\varepsilon_{ri} k_o^2 - \beta^2)\phi^e_{yi} = 0 \qquad (5b)$$

where $k_o^2 = \omega^2 \mu_o \varepsilon_o$ is the free space wavenumber and ε_{ri} is the relative dielectric constant in region i. In homogeneous source-free regions, the electromagnetic field in terms of $\vec{\phi}^h_i$ and $\vec{\phi}^e_i$ is given [26] by :

$$\vec{E}_i = -\nabla \times \vec{\phi}^h_i + \frac{1}{\hat{y}} \nabla \times \nabla \times \vec{\phi}^e_i \qquad (6a)$$

$$\vec{H}_i = \nabla \times \vec{\phi}^e_i + \frac{1}{\hat{z}} \nabla \times \nabla \times \vec{\phi}^h_i \qquad (6b)$$

where $\hat{y}_i = j\omega\varepsilon_{ri}\varepsilon_o$ and $\hat{z}_i = j\omega\mu_o$.

After taking the Fourier transforms of equation (5), we obtain solutions for the transformed quantities $\hat{\phi}^h_{yi}(\alpha,y)$ and $\hat{\phi}^e_{yi}(\alpha,y)$:

$$\hat{\phi}^h_{y1}(\alpha,y) = A^h e^{-\gamma_1(y-d)} \quad ; \quad d < y \qquad (7a)$$

$$\hat{\phi}^e_{y1}(\alpha,y) = A^e e^{-\gamma_1(y-d)} \quad ; \quad d < y \qquad (7b)$$

$$\hat{\phi}^h_{y2}(\alpha,y) = B^h \sinh \gamma_2 y \quad ; \quad 0 < y < d \qquad (7c)$$

$$\hat{\phi}^e_{y2}(\alpha,y) = B^e \cosh \gamma_2 y \quad ; \quad 0 < y < d \qquad (7d)$$

$$\gamma_1 = \sqrt{\alpha^2 + \beta^2 - k_o^2}$$

$$\gamma_2 = \sqrt{\alpha^2 + \beta^2 - \varepsilon_r k_o^2}$$

where A^h, A^e, B^h and B^e are unknown coefficients. The boundary condition of the perfectly conducting plane at y = 0 is embedded in this set of solutions. Also, γ_1 is chosen to be positive so that the radiation condition at y = ∞ is satisfied. Substitution of these solutions into the Fourier transforms of equations (6a,b) yields the field expressions in both regions:

Region I (y > d):

$$E_{x1} = \left[-j\beta A^h + j\alpha \frac{\gamma_1}{\hat{y}_1} A^e \right] e^{-\gamma_1 (y-d)} \qquad (8a)$$

$$E_{y1} = \left[-\hat{z}_1 + \frac{\gamma_1^2}{\hat{y}_2} \right] A^e \, e^{-\gamma_1 (y-d)} \qquad (8b)$$

$$E_{z1} = \left[j\alpha A^h + j\beta \frac{\gamma_1}{\hat{z}} A^e \right] e^{-\gamma_1 (y-d)} \qquad (8c)$$

$$H_{x1} = \left[j\beta A^e + j\alpha \frac{\gamma_1}{\hat{y}_1} A^h \right] e^{-\gamma_1 (y-d)} \qquad (8d)$$

$$H_{y1} = \left[-\hat{y}_1 + \frac{\gamma_1^2}{\hat{z}_1} \right] A^h \, e^{-\gamma_1 (y-d)} \qquad (8e)$$

$$H_{z1} = \left[-j\alpha A^e + j\beta \frac{\gamma_1}{\hat{z}_1} A^h \right] e^{-\gamma_1 (y-d)} \qquad (8f)$$

Region II ($0 < y < d$)

$$E_{x2} = \left[-j\beta B^h - j\alpha \frac{\gamma_2}{\hat{y}_2} B^e \right] \sinh \gamma_2 y \qquad (9a)$$

$$E_{y2} = \left[-\hat{z}_2 + \frac{\gamma_2^2}{\hat{y}_2} \right] B^e \cosh \gamma_2 y \qquad (9b)$$

$$E_{z2} = \left[j\alpha B^h - j\beta \frac{\gamma_2}{\hat{y}_2} B^e \right] \sinh \gamma_2 y \qquad (9c)$$

$$H_{x2} = \left[j\beta B^e - j\alpha \frac{\gamma_2}{\hat{y}_2} B^h \right] \cosh \gamma_2 y \qquad (9d)$$

$$H_{y2} = \left[-\hat{y}_2 + \frac{\gamma_2^2}{\hat{z}_2} \right] B^h \sinh \gamma_2 y \qquad (9e)$$

$$H_{z2} = \left[-j\alpha B^e - j\beta \frac{\gamma_2}{\hat{z}_2} B^h \right] \cosh \gamma_2 y \qquad (9f)$$

Finally, the boundary conditions at $y = d$ have to be satisfied. In the spectral (or Fourier transform) domain, the boundary conditions are:

$$\tilde{E}_{x1}(\alpha) = \tilde{E}_{x2}(\alpha) = \tilde{E}_x(\alpha) \qquad (10a)$$

$$\tilde{E}_{z1}(\alpha) = \tilde{E}_{z2}(\alpha) = \tilde{E}_z(\alpha) \qquad (10b)$$

$$\tilde{H}_{x2}(\alpha) - \tilde{H}_{x1}(\alpha) = \tilde{J}_z(\alpha) \qquad (10c)$$

$$\tilde{H}_{z2}(\alpha) - \tilde{H}_{z1}(\alpha) = -\tilde{J}_x(\alpha) \qquad (10d)$$

where $\tilde{J}_z$ and $\tilde{J}_x$ are Fourier transforms of unknown current components J_z and J_x on the conducting region at $y = d$. These conditions allow us to obtain the expressions for coefficients A^h, A^e, B^h and B^e in terms of $\tilde{J}_z$ and $\tilde{J}_x$:

$$A^h = B^h \sinh \gamma_2 d = j \frac{1}{\frac{\gamma_1}{\hat{z}_1} + \frac{\gamma_2}{\hat{z}_2} \coth \gamma_2 d} \cdot \frac{\alpha \tilde{J}_z - \beta \tilde{J}_x}{\alpha^2 + \beta^2} \qquad (11a)$$

$$\frac{\gamma_1}{\hat{y}_1} A^e = -\frac{\gamma_2}{\hat{y}_2} B^e \sinh \gamma_2 d = -j \frac{1}{\frac{\hat{y}_1}{\gamma_1} + \frac{\hat{y}_2}{\gamma_2} \coth \gamma_2 d} \cdot \frac{\beta \tilde{J}_z + \alpha \tilde{J}_x}{\alpha^2 + \beta^2} \qquad (11b)$$

By substituting equations (11a,b) into (8a) and (8c), we obtain the algebraic equations (2a,b) with the Green's admittance functions $\tilde{Y}_{zz}$, etc., expressed in closed forms as follows:

$$\tilde{Y}_{zz} = \frac{\alpha^2}{\alpha^2 + \beta^2} \left(\frac{\gamma_1}{\hat{z}_1} + \frac{\gamma_2}{\hat{z}_2} \coth \gamma_2 d \right) + \frac{\beta^2}{\alpha^2 + \beta^2} \left(\frac{\hat{y}_1}{\gamma_1} + \frac{\hat{y}_2}{\gamma_2} \coth \gamma_2 d \right) \qquad (12a)$$

$$\tilde{Y}_{zx} = \tilde{Y}_{xz} = \frac{\alpha\beta}{\alpha^2 + \beta^2} \left(\frac{\hat{y}_1}{\gamma_1} + \frac{\hat{y}_2}{\gamma_2} \coth \gamma_2 d - \frac{\gamma_1}{\hat{z}_1} - \frac{\gamma_2}{\hat{z}_2} \coth \gamma_2 d \right) \qquad (12b)$$

$$\tilde{Y}_{xx} = \frac{\beta^2}{\alpha^2 + \beta^2} \left(\frac{\gamma_1}{\hat{z}_1} + \frac{\gamma_2}{\hat{z}_2} \coth \gamma_2 d \right) + \frac{\alpha^2}{\alpha^2 + \beta^2} \left(\frac{\hat{y}_1}{\gamma_1} + \frac{\hat{y}_2}{\gamma_2} \coth \gamma_2 d \right) \qquad (12c)$$

This process of formulating the Green's functions is straightforward but rather lengthy, especially when more dielectric layers are used. Therefore, a simpler method of formulation proposed by Itoh [24] will be discussed. This new method is fast and easy while it gives more physical insight of the spectral domain method.

From the form of the inverse Fourier transform

$$\phi(x,y)\, e^{-j\beta z} = \frac{1}{\sqrt{2\pi}} \int_{-\infty}^{\infty} \tilde{\phi}\,(\alpha,y)\, e^{-j(\alpha x + \beta z)}\, d\alpha \qquad (13)$$

we recognize that the field components in the space domain are the superposition of nonuniform plane waves (spectral waves) propagating in the direction of θ from the z-axis, where $\theta = \cos^{-1}(\beta/\sqrt{\alpha^2 + \beta^2})$. For convenience, we define in Fig. 5 a u,v-coordinate system for each spectral wave, which has a rotational relation with the x,z-coordinate system defined by

$$u = x\cos\theta - z\sin\theta \qquad (14a)$$

$$v = x\sin\theta + z\cos\theta \qquad (14b)$$

For each θ (i.e., for each α), the nonuniform plane wave may be decomposed into TM-to-y ($\tilde{E}_y$, $\tilde{E}_v$, $\tilde{H}_u$) and TE-to-y ($\tilde{H}_y$, $\tilde{E}_u$, $\tilde{H}_v$) surface waves for which homogeneous boundary conditions apply. Since the spectral current $\tilde{J}_v$ is due only to the discontinuity of the tangential $\tilde{H}_u$ component in the TM fields, and $\tilde{J}_u$ is due only to TE fields, they can be dealt with independently.

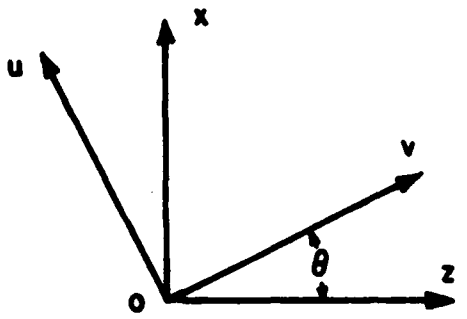

$$\sin\theta = \frac{\alpha}{\sqrt{\alpha^2+\beta^2}} \; ; \; \cos\theta = \frac{\beta}{\sqrt{\alpha^2+\beta^2}}$$

Fig. 5. Coordinate transformation.

For surface wave modes, the characteristic equations may be obtained from the transverse resonance conditions of the equivalent transmission line circuits. Fig. 6 shows the equivalent circuits for both TM and TE cases. The characteristic admittances in each region are

$$Y_{TMi} = \frac{\tilde{H}_{ui}}{\tilde{E}_{vi}} = \frac{\hat{y}_i}{\gamma_i} \quad ; \quad i = 1,2 \qquad (15a)$$

$$Y_{TEi} = -\frac{\tilde{H}_{vi}}{\tilde{E}_{ui}} = \frac{\gamma_i}{\hat{z}_i} \quad ; \quad i = 1,2 \qquad (15b)$$

where $\gamma_i = \sqrt{\alpha^2 + \beta^2 - \varepsilon_{ri} k_o^2}$ is the propagation constant in the y direction in the i-th region. All the boundary conditions for the TE and TM waves are readily incorporated in the equivalent circuits. For instance, the conducting plane at y = 0 is represented by a short circuit. The electric fields $\tilde{E}_v$ and $\tilde{E}_u$ are continuous at y = d and are related to the currents via

$$\tilde{J}_v(\alpha) = \tilde{Y}^e(\alpha,\beta)\ \tilde{E}_v(\alpha) \qquad (16a)$$

$$\tilde{J}_u(\alpha) = \tilde{Y}^h(\alpha,\beta)\ \tilde{E}_u(\alpha) \qquad (16b)$$

$\tilde{Y}^e$ and $\tilde{Y}^h$ are the input admittances looking into the equivalent circuits from the current sources at y = d, and are given by

$$\tilde{Y}^e(\alpha,\beta) = Y_1^e + Y_2^e \qquad (17a)$$

$$\tilde{Y}^h(\alpha,\beta) = Y_1^h + Y_2^h \qquad (17b)$$

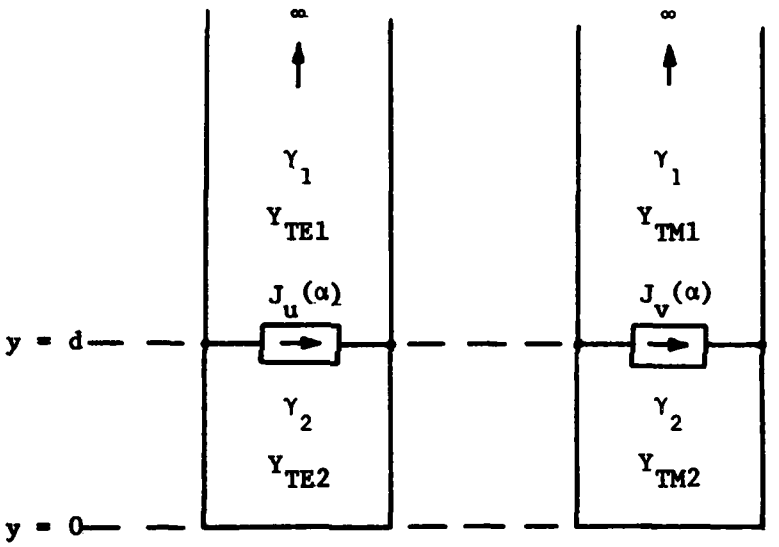

Fig. 6. Transverse equivalent circuits for conductor-backed coplanar waveguide.

where Y_1^e and Y_2^e are the input admittances looking upward and downward, respectively, at y = d in the TM equivalent circuit, and Y_1^h and Y_2^h are input admittances in the TE circuit:

$$Y_1^e = Y_{TM1} \quad , \quad Y_2^e = Y_{TM2} \coth \gamma_2 d \qquad (18a)$$

$$Y_1^h = Y_{TE1} \quad , \quad Y_2^h = Y_{TE2} \coth \gamma_2 d \qquad (18b)$$

The final step is to derive the relation (2a,b) in the x,z-coordinate system from equations (16a,b) via a coordinate transformation. Because the transformation is a simple coordinate rotation (14), $\tilde{E}_x$ and $\tilde{E}_z$ ($\tilde{J}_x$ and $\tilde{J}_z$) are linear combinations of $\tilde{E}_u$ and $\tilde{E}_v$ ($\tilde{J}_u$ and $\tilde{J}_v$). After the transformation, the admittance matrix elements in (2) are found to be

$$\tilde{Y}_{zz}(\alpha,\beta) = \sin^2\theta\, \tilde{Y}^h + \cos^2\theta\, \tilde{Y}^e \qquad (19a)$$

$$\tilde{Y}_{zx}(\alpha,\beta) = \tilde{Y}_{xz}(\alpha,\beta) = \sin\theta \cos\theta\, (\tilde{Y}^e - \tilde{Y}^h) \qquad (19b)$$

$$\tilde{Y}_{xx}(\alpha,\beta) = \cos^2\theta\, \tilde{Y}^h + \sin^2\theta\, \tilde{Y}^e \qquad (19c)$$

where

$$\sin\theta = \frac{\alpha}{\sqrt{\alpha^2 + \beta^2}} \quad , \quad \cos\theta = \frac{\beta}{\sqrt{\alpha^2 + \beta^2}}$$

It is easily shown that this equation is identical to equation (12).

Now that we have derived the equations correspond the integral equations (1a,b), with closed form expressi the Green's functions in the spectral domain, the solution phase constant β in the z-direction is to be calculated. T end, Galerkin's method is applied by expanding the electric components $\tilde{E}_x$ and $\tilde{E}_z$ in terms of known basis functions $\tilde{E}_{xn}$ as follows:

$$\tilde{E}_z(\alpha) = \sum_{n=1}^{N} d_n \tilde{E}_{zn}(\alpha)$$

$$\tilde{E}_x(\alpha) = \sum_{n=0}^{M} c_n \tilde{E}_{xn}(\alpha)$$

where c_n and d_n are unknown coefficients. The basis functi and $\tilde{E}_{zn}$ must be chosen such that their inverse Fourier tran are nonzero only in the slots. After substituting (II-20) (II-2) and taking the inner products of the resultant equat with the basis functions $\tilde{E}_{xn}$ and $\tilde{E}_{zn}$, we obtain the linear taneous equations:

$$\sum_{n=0}^{M} K_{mn}^{(1,1)} c_n + \sum_{n=1}^{N} K_{mn}^{(1,2)} d_n = 0 \quad , \quad m = 0,1...M$$

$$\sum_{n=0}^{M} K_{mn}^{(2,1)} c_n + \sum_{n=1}^{N} K_{mn}^{(2,2)} d_n = 0 \quad , \quad m = 1,2...N$$

where

$$K_{mn}^{(1,1)} = \int_{-\infty}^{\infty} \tilde{E}_{zm}(\alpha) \tilde{Y}_{zz}(\alpha,\beta) \tilde{E}_{zn}(\alpha) \, d\alpha$$

$$K_{mn}^{(1,2)} = \int_{-\infty}^{\infty} \tilde{E}_{zm}(\alpha)\, \tilde{Y}_{zx}(\alpha,\beta)\, \tilde{E}_{xn}(\alpha)\, d\alpha$$

$$K_{mn}^{(2,1)} = \int_{-\infty}^{\infty} \tilde{E}_{xm}(\alpha)\, \tilde{Y}_{xz}(\alpha,\beta)\, \tilde{E}_{zn}(\alpha)\, d\alpha$$

$$K_{mn}^{(2,2)} = \int_{-\infty}^{\infty} \tilde{E}_{xm}(\alpha)\, \tilde{Y}_{xx}(\alpha,\beta)\, \tilde{E}_{xn}(\alpha)\, d\alpha$$

Notice that the right hand sides of (2a,b) are eliminated by this procedure. This can be verified by using Parseval's theorem that

$$\int_{-\infty}^{\infty} \tilde{E}_{zm}(\alpha)\, \tilde{J}_z(\alpha)\, d\alpha = \int_{-\infty}^{\infty} E_{zm}(x)\, J_z(x) = 0 \qquad (22)$$

The above relation is true since $E_{zm}(x)$ [the inverse transform of $\tilde{E}_{zm}(\alpha)$] and $J_z(x)$ are nonzero in the complementary regions of x at y = d.

Finally, the propagation constant β is obtained by solving the system of simultaneous equations, (21). Since this set of equations is homogeneous, non-trivial solutions can be obtained only when the determinant of its coefficient matrix is equal to zero, i.e., the matrix is singular. This results in a characteristic equation, from which β is obtained.

B. Characteristic Impedance

Due to the non-TEM nature of the conductor-backed coplanar waveguide, the definition of characteristic impedance is not unique. One possible choice is to define it as

$$Z_c = \frac{V_o^2}{2P_{avg}} \qquad (23)$$

where V_o is the slot voltage and P_{avg} is the time-average power flow on the line, which is given by

$$P_{avg} = R_e \iint_{-\infty}^{\infty} \vec{E} \times \vec{H}^* \cdot \vec{a}_z \, dxdy \qquad (24)$$

Since the limits of integration are infinite, Paseval's theorem may be used to transform the expression into the spectral domain as

$$P_{avg} = R_e \iint_{-\infty}^{\infty} [\tilde{E}_x(\alpha,y) \tilde{H}_y^*(\alpha,y) - \tilde{E}_y(\alpha,y) \tilde{H}_x^*(\alpha,y)] \, dxdy \qquad (25)$$

Expressions for the electric and magnetic fields in both regions are given by equations (8) and (9). Since the y-dependence of these expressions is simple, the integration with respect to y may be performed analytically. (25) then becomes a single integral of the form

$$P_{avg} = R_e \int_{-\infty}^{\infty} g(\alpha) \, d\alpha \qquad (26)$$

where

$$g(\alpha) = j\frac{1}{2}\left(\frac{\hat{y}_1}{\gamma_1} - \frac{\gamma_1}{\hat{z}_1}\right)\left[2\alpha\bar{\bar{C}}\bar{\bar{D}} + \beta\left(\frac{\hat{y}_1}{\gamma_1}\,\frac{\hat{z}_1}{\gamma_1}\,\bar{\bar{C}}^2 - \bar{\bar{D}}^2\right)\right]$$

$$+ j\frac{1}{2}\frac{\beta\gamma_2 d}{\sinh^2 \gamma_2 d}\left(\frac{\hat{y}_2}{\gamma_2} - \frac{\gamma_2}{\hat{z}_2}\right)\left(\bar{\bar{D}}^2 + \frac{\hat{y}_2}{\gamma_2}\,\frac{\hat{z}_2}{\gamma_2}\,\bar{\bar{C}}^2\right)$$

$$+ j \frac{1}{2} \coth \gamma_2 d \left(\frac{\hat{y}_2}{\gamma_2} - \frac{\gamma_2}{\hat{z}_2} \right) \left[2\alpha\bar{C}\bar{D} + \beta \left(\frac{\hat{y}_2}{\gamma_2} \frac{\hat{z}_2}{\gamma_2} \bar{C}^2 - \bar{D}^2 \right) \right]$$

$$\bar{C} = \frac{\beta \hat{E}_z + \alpha \hat{E}_x}{\alpha^2 + \beta^2}$$

$$\bar{D} = \frac{\alpha \hat{E}_z - \beta \hat{E}_x}{\alpha^2 + \beta^2}$$

Note that the calculation of these expressions requires the value of $\hat{E}_z$ and $\hat{E}_x$ be known, i.e., the expansion coefficients c_n and d_n be obtained by solving the equations (21a,b) for a known β.

Finally, the voltage V_o is computed. This involves simply the integration of the assumed electric field distribution across the slot and can be done analytically. However, the evaluation of (26) must be done on a digital computer.

C. Choice of Basis Functions

Any kind of basis function may be used as long as it is nonzero only in the slot regions. However, due to the variational nature of the approach, the efficiency and accuracy of this method depend greatly on the choice of basis functions. In this study, the basis functions are selected in accordance with the following criteria:

1) For rapid convergence of the solution the functions should satisfy the edge condition [27] which requires that $E_z(x)$ behaves like

$|x - x_e|^{1/2}$ near the edge x_e of a strip, whereas $E_x(x)$ approaches x_e with the singularity $|x - x_e|^{-1/2}$.

2) The set of functions E_{xi}, E_{zi} should be complete to enable approximation of the exact solution to any degree desired simply by increasing the number of terms of the expansion. In this way the numerical solutions can be easily checked for their convergence.

3) All the physical insight available should be incorporated into the choice of expansion functions so that the combination of them can closely represent a modal field distribution and the matrix size can be held small for the given required accuracy.

4) It is desirable that the transforms $\tilde{E}_{xi}$ $\tilde{E}_{zi}$ are available in a fairly simple analytical form.

With the above considerations in mind, the following set of functions are employed [28]

$$E_{xn}(x) = \begin{cases} \dfrac{\cos \frac{n\pi}{2w} x}{\sqrt{w^2 - x^2}} & \text{for } n = 0,2,4... \\ \dfrac{\sin \frac{n\pi}{2w} x}{\sqrt{w^2 - x^2}} & \text{for } n = 1,3,5... \end{cases} \qquad (27a)$$

$$E_{zn}(x) = \begin{cases} \dfrac{\cos \frac{n\pi}{2w} x}{\sqrt{w^2 - x^2}} & \text{for } n = 1,3,5... \\ \dfrac{\sin \frac{n\pi}{2w} x}{\sqrt{w^2 - x^2}} & \text{for } n = 2,4,6... \end{cases} \qquad (27b)$$

Note that these functions are defined only over one slot. For even mode solutions, complete figures for the first three basis functions are shown in Fig. 7. The Fourier transforms of the entire set are

$$\tilde{E}_{xn}(\alpha) = \begin{cases} j\sqrt{\frac{\pi}{2}} \sin b\alpha \left[J_o(|w\alpha + \frac{n\pi}{2}|) + J_o(|w\alpha - \frac{n\pi}{2}|) \right] \\ \qquad ; \text{ for } n = 0,2,4,... \\ -j\sqrt{\frac{\pi}{2}} \cos b\alpha \left[J_o(|w\alpha + \frac{n\pi}{2}|) - J_o(|w\alpha - \frac{n\pi}{2}|) \right] \\ \qquad ; \text{ for } n = 1,3,5,... \end{cases} \qquad (28a)$$

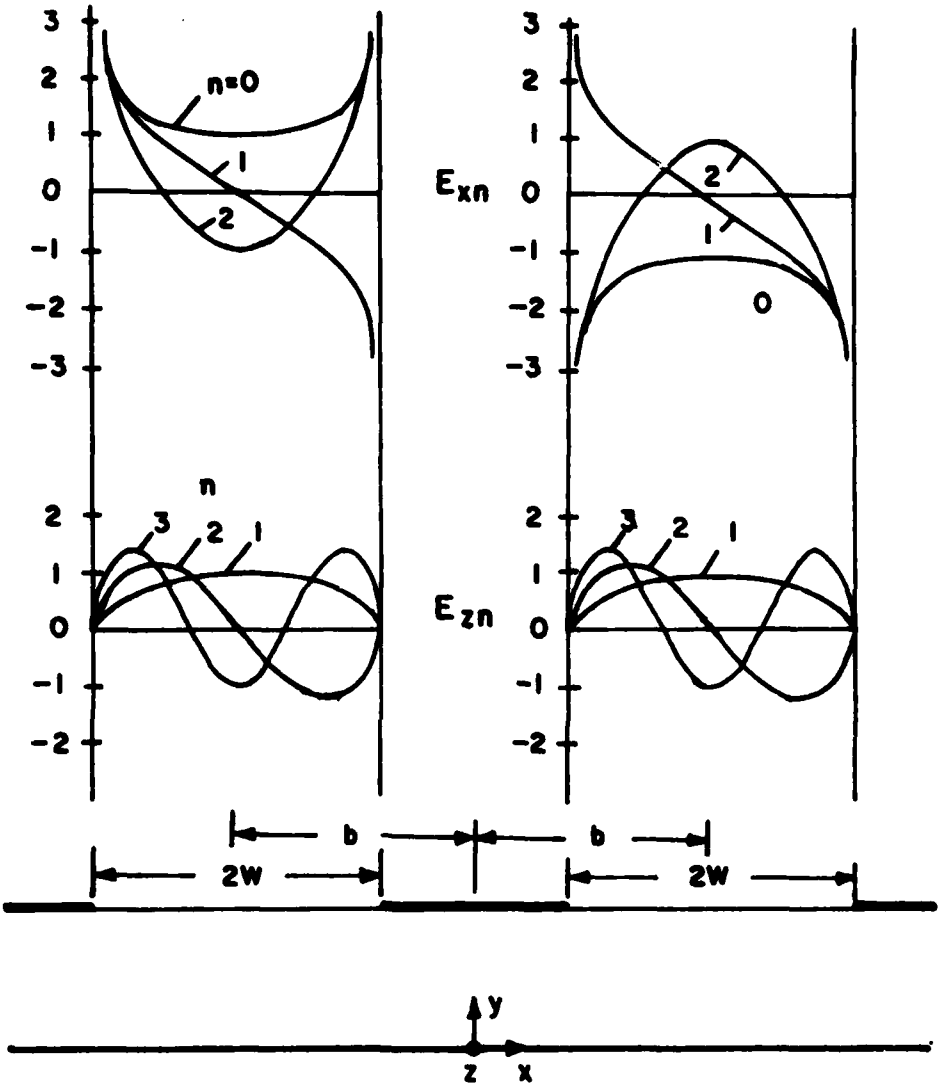

Fig. 7. Field distribution of the first three basis functions.

$$\tilde{E}_{zn}(\alpha) = \begin{cases} \sqrt{\frac{\pi}{2}} \cos b\alpha \left[J_o(|w\alpha + \frac{n\pi}{2}|) + J_o(|w\alpha - \frac{n\pi}{2}|) \right] \\ \qquad\qquad ; \text{ for } n = 1,3,5,\ldots \qquad (28b) \\ \sqrt{\frac{\pi}{2}} \sin b\alpha \left[J_o(|w\alpha + \frac{n\pi}{2}|) - J_o(|w\alpha - \frac{n\pi}{2}|) \right] \\ \qquad\qquad ; \text{ for } n = 2,4,6,\ldots \end{cases}$$

where J_o denotes the zero-order Bessel function of the first kind.

D. MIS Slow-wave Structures

For the MIS structures, the analysis is more involved due to the presence of a lossy semiconductor layer with a relatively high conductivity. The phase constant and the bulk attenuation can no longer be calculated by means of a perturbation theory as for the low-loss case. The losses must be taken into account during the formulation. This is done by employing a complex permittivity $\epsilon^* = \epsilon' - j\epsilon''$ in the lossy region, where $\epsilon'' = \frac{\sigma}{\omega}$ contains the conductivity information of the lossy material. The rest of the formulation follows very closely the process described in Section II, B. For convenience of analysis the cross-sectional views of the MIS coplanar waveguide and microstrip line are shown in Fig. 8 together with their equivalent circuits.

The Green's admittance functions for the coplanar waveguide are of the same form as (19), where the input admittances looking into the equivalent circuits are given by

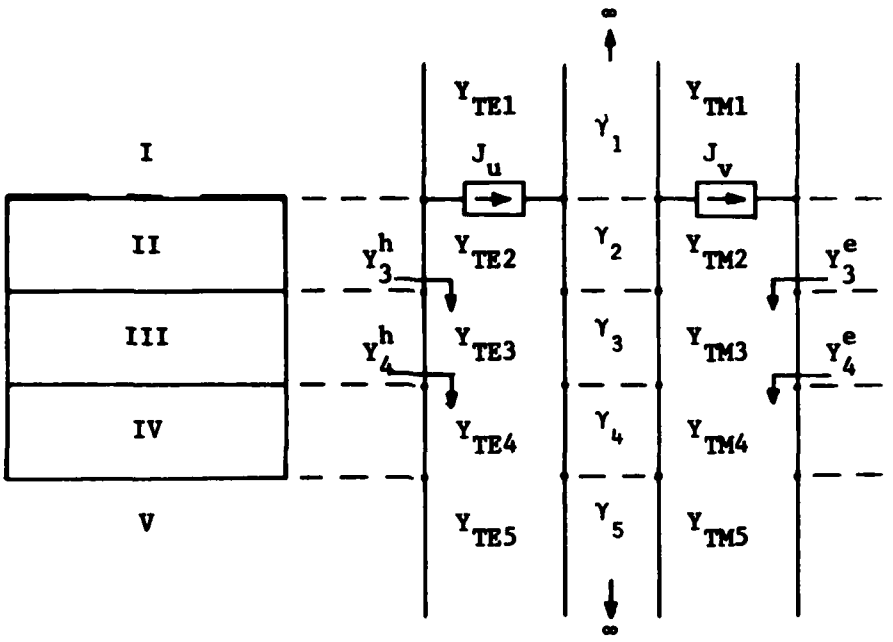

(a)

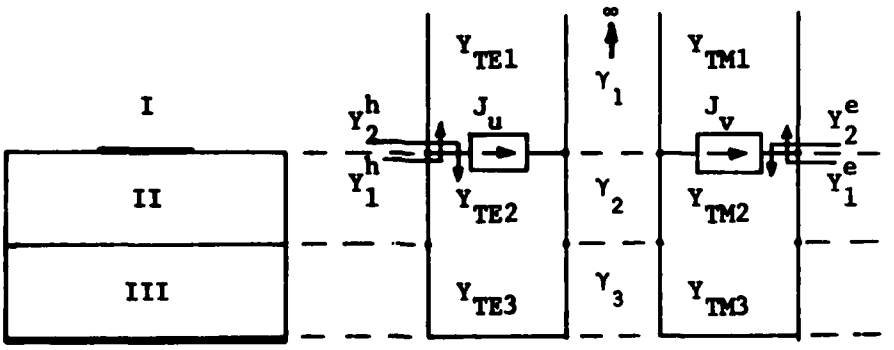

(b)

Fig. 8. Transverse equivalent circuits. (a) Coplanar waveguide, (b) Microstrip lines.

$$\hat{Y}^e = \frac{\hat{y}_1}{\gamma_1} + \frac{\hat{y}_2}{\gamma_2} \cdot \frac{Y_3^e + \frac{\hat{y}_2}{\gamma_2} \tanh \gamma_2 d_2}{\frac{\hat{y}_2}{\gamma_2} + Y_3^e \tanh \gamma_2 d_2} \qquad (29a)$$

$$\hat{Y}^h = \frac{\gamma_1}{\hat{z}_1} + \frac{\gamma_2}{\hat{z}_2} \cdot \frac{Y_3^h + \frac{\gamma_2}{\hat{z}_2} \tanh \gamma_2 d_2}{\frac{\gamma_2}{\hat{z}_2} + Y_3^h \tanh \gamma_2 d_2} \qquad (29b)$$

with

$$Y_3^e = \frac{\hat{y}_3}{\gamma_3} \cdot \frac{Y_4^e + \frac{\hat{y}_3}{\gamma_3} \tanh \gamma_3 d_3}{\frac{\hat{y}_3}{\gamma_3} + Y_4^e \tanh \gamma_3 d_3} \quad ; \quad Y_3^h = \frac{\gamma_3}{\hat{z}_3} \cdot \frac{Y_4^h + \frac{\gamma_3}{\hat{z}_3} \tanh \gamma_3 d_3}{\frac{\gamma_3}{\hat{z}_3} + Y_4^h \tanh \gamma_3 d_3}$$

$$Y_4^e = \frac{\hat{y}_4}{\gamma_4} \cdot \frac{\frac{\hat{y}_5}{\gamma_5} + \frac{\hat{y}_4}{\gamma_4} \tanh \gamma_4 d_4}{\frac{\hat{y}_4}{\gamma_4} + \frac{\hat{y}_5}{\gamma_5} \tanh \gamma_4 d_4} \quad ; \quad Y_4^h = \frac{\gamma_4}{\hat{z}_4} \cdot \frac{\frac{\gamma_5}{\hat{z}_5} + \frac{\gamma_4}{\hat{z}_4} \tanh \gamma_4 d_4}{\frac{\gamma_4}{\hat{z}_4} + \frac{\gamma_5}{\hat{z}_5} \tanh \gamma_4 d_4}$$

The same set of basis functions as in (28) are used in the Galerkin's procedure. A complex propagation constant, which is composed of the imaginary phase constant and real attenuation constant, is obtained by a root-seeking computer program.

In the analysis of the MIS microstrip line, the basis function expansion is more easily performed over the current components on the finite strip, rather than the electric fields that extend to infinity. To do this, the formulation process is

modified. Instead of equation (2), the following equations are obtained

$$\tilde{Z}_{zz}(\alpha,\beta)\ \tilde{J}_z(\alpha) + \tilde{Z}_{zx}(\alpha,\beta)\ \tilde{J}_x(\alpha) = \tilde{E}_z(\alpha) \qquad (30a)$$

$$\tilde{Z}_{xz}(\alpha,\beta)\ \tilde{J}_z(\alpha) + \tilde{Z}_{xx}(\alpha,\beta)\ \tilde{J}_x(\alpha) = \tilde{E}_x(\alpha) \qquad (30b)$$

where $\tilde{Z}_{zz}$, $\tilde{Z}_{zx}$, $\tilde{Z}_{xz}$ and $\tilde{Z}_{xx}$ are the Green's impedance functions given as follows:

$$\tilde{Z}_{zz}(\alpha,\beta) = \frac{\beta^2}{\alpha^2+\beta^2}\,\tilde{Z}^e + \frac{\alpha^2}{\alpha^2+\beta^2}\,\tilde{Z}^h \qquad (31a)$$

$$\tilde{Z}_{zx}(\alpha,\beta) = \tilde{Z}_{xz}(\alpha,\beta) = \frac{\alpha\beta}{\alpha^2+\beta^2}\,(\tilde{Z}^e - \tilde{Z}^h) \qquad (31b)$$

$$\tilde{Z}_{xx}(\alpha,\beta) = \frac{\alpha^2}{\alpha^2+\beta^2}\,\tilde{Z}^e + \frac{\beta^2}{\alpha^2+\beta^2}\,\tilde{Z}^h \qquad (31c)$$

with

$$\tilde{Z}^e = \left[Y_1^e + Y_2^e\right]^{-1} = \left[\frac{\hat{y}_1}{\gamma_1} + \frac{\hat{y}_2}{\gamma_2}\ \frac{\frac{\hat{y}_3}{\gamma_3} + \frac{\hat{y}_2}{\gamma_2}\tanh\gamma_2 d_2}{\frac{\hat{y}_2}{\gamma_2} + \frac{\hat{y}_3}{\gamma_3}\tanh\gamma_2 d_2}\right]^{-1} \qquad (31d)$$

$$\tilde{Z}^h = \left[Y_1^h + Y_2^h\right]^{-1} = \left[\frac{\gamma_1}{\hat{z}_1} + \frac{\gamma_2}{\hat{z}_2}\ \frac{\frac{\gamma_3}{\hat{z}_3} + \frac{\gamma_2}{\hat{z}_2}\tanh\gamma_2 d_2}{\frac{\gamma_2}{\hat{z}_2} + \frac{\gamma_3}{\hat{z}_3}\tanh\gamma_2 d_2}\right]^{-1} \qquad (31e)$$

Since the slot E-fields and strip currents have analogous properties, the expressions for E_{xn} and E_{zn} are used for J_{zn} and J_{xn}, respectively. For fundamental mode studies only even-symmetric

J_{zn} and odd-symmetric J_{xz} are used. Their Fourier transforms are

$$\tilde{J}_{zn}(\alpha) = \frac{1}{2}\sqrt{\frac{\pi}{2}}\,[J_o(|w\alpha + n\pi|) + J_o(|w\alpha - n\pi|)] \quad ; \quad n = 0,1,2,... \tag{32a}$$

$$\tilde{J}_{xn}(\alpha) = \frac{1}{2j}\sqrt{\frac{\pi}{2}}\,[J_o(|w\alpha + n\pi|) - J_o(|w\alpha - n\pi|)] \quad , \quad n = 1,2,3,... \tag{32b}$$

III. RESULTS AND DISCUSSION

A. Conductor-Backed Coplanar Waveguide

The conductor-backed coplanar waveguide has been studied for a wide range of geometric parameters. Fig. 9 shows typical results of the dispersion property, assuming GaAs as the substrate ($\varepsilon_r = 13.0$). Aspect ratios a/d and w/d are the parameters varied. Since the present structure is a mixture of a microstrip line and a coplanar waveguide, the properties of either one become predominant depending on the structural parameters. As the slot width increases for a fixed substrate thickness, the characteristic approaches that of a microstrip line. This behavior is shown in Fig. 9a. On the other hand, when the slot width is fixed and the thickness increases, the behavior approaches the coplanar waveguide case, as depicted in Fig. 9b.

For a moderate aspect ratio (e.g., a/d = 1/3, w/d = 1/3), the transmission line becomes less dispersive than the corresponding microstrip line with the same aspect ratio (a/d = 1/3). This suggests that we may define the characteristic impedance of the

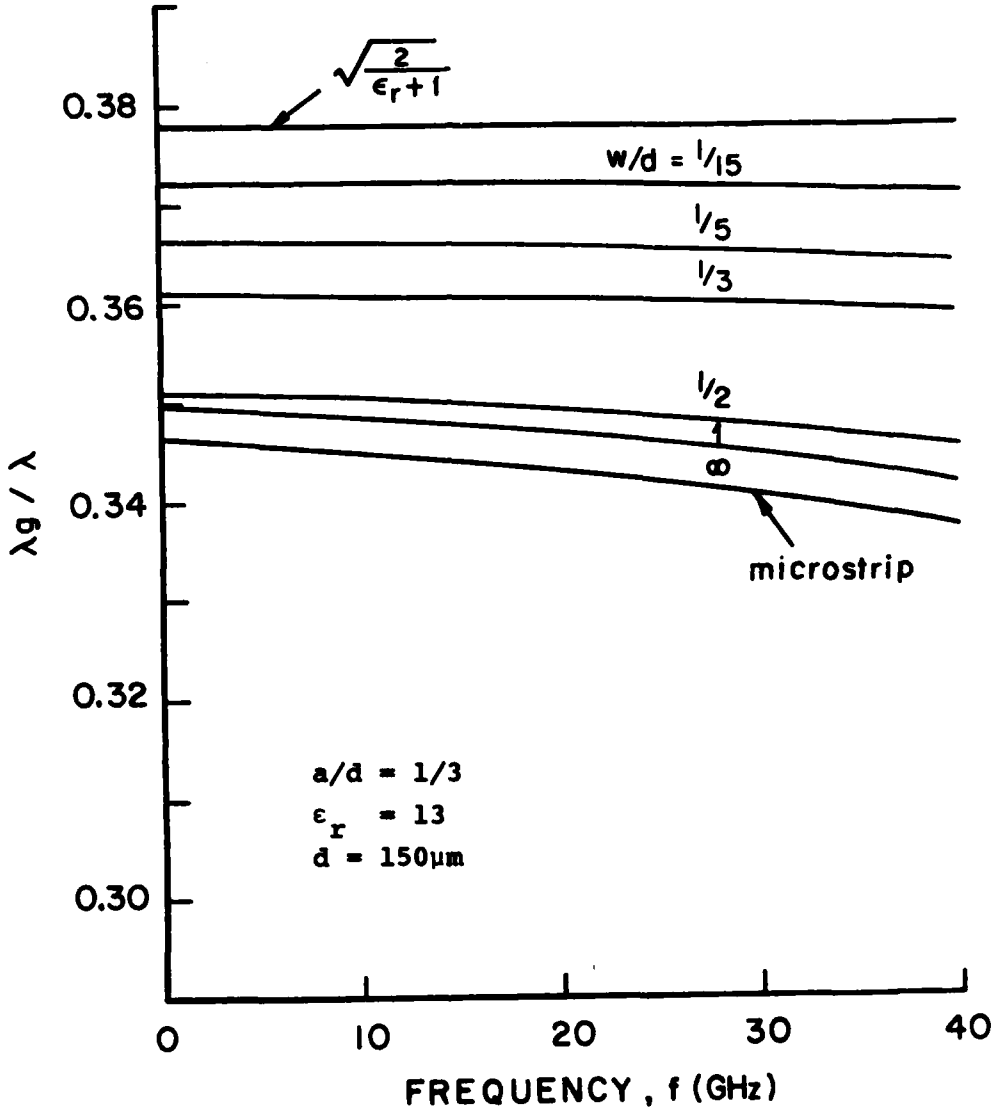

Fig. 9a. Dispersion characteristics of conductor-backed coplanar waveguide.

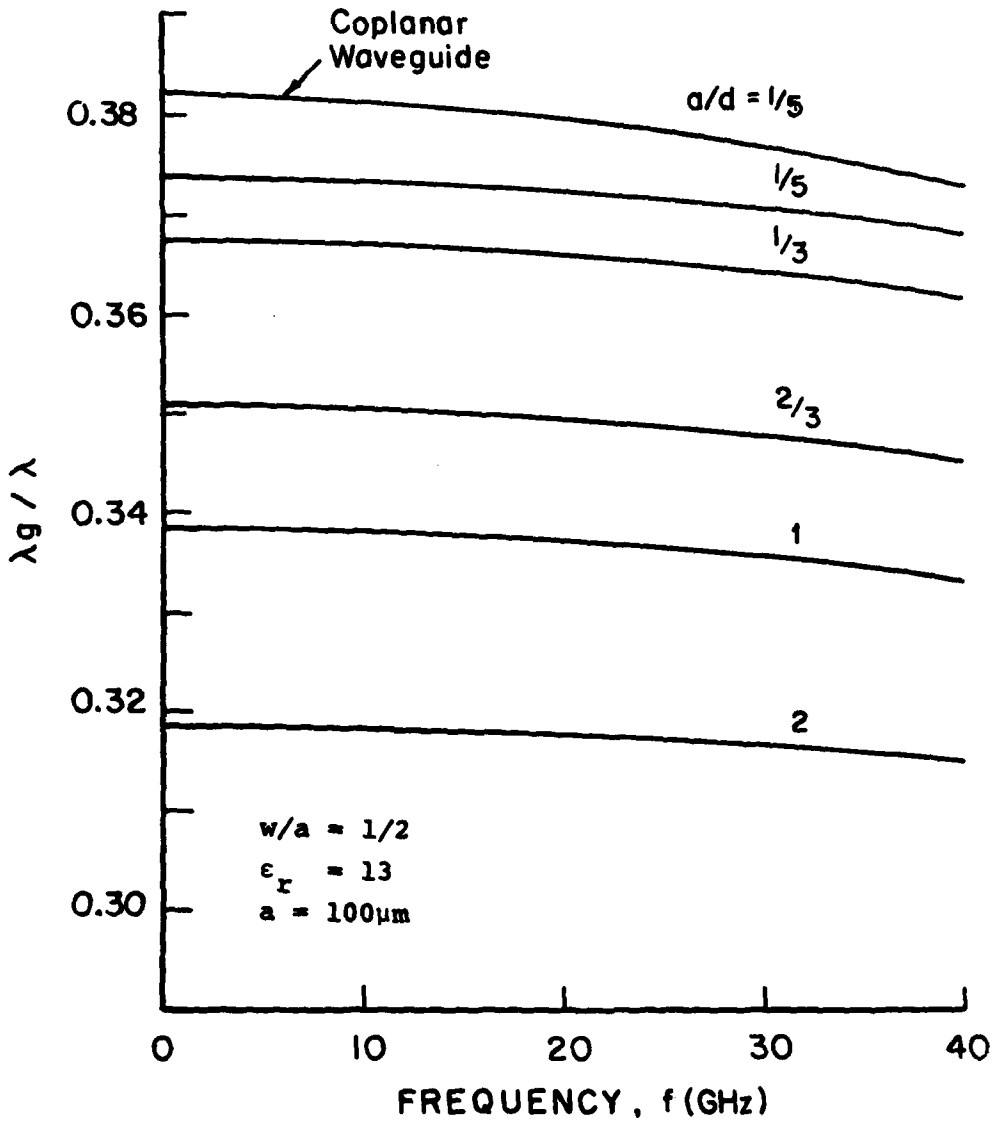

Fig. 9b. Dispersion characteristics of conductor-backed coplanar waveguide.

transmission line as $Z_c = Z_o/\sqrt{\varepsilon_{eff}}$, where ε_{eff} is the effe dielectric constant defined as $(\beta/k)^2$ and Z_o is the charac impedance when $\varepsilon_r = 1$. The impedance Z_c computed in this plotted in Fig. 10. It is observed that the characteri impedance decreases as the slot widths decrease, while the constant is relatively unaffected. Therefore, by adjustin center strip width and slot widths, one can have independe of the phase constant and the characteristic impedance. F substrate, the usable practical impedance range is approxi 15-120 Ω.

The number of basis functions required for accur largely dependent on the aspect ratios. For small w/a and only E_{xo} is required since both the slot coupling effect a effect of the ground-backing are small. For larger w/a, E_x needed to represent the stronger coupling effect between t Finally, when the thickness becomes comparable to the slot more basis functions are required for accurate results. I study, up to seven basis functions have been used for some cases. The computation time for such a solution is about on a CDC Dual Cyber 170/750.

B. MIS Microstrip Lines

An experimental study on the properties of micrc lines formed on a Si-SiO_2 system has been done by Hasegawa [18]. Their structure is the one in Fig. 8b with SiO_2

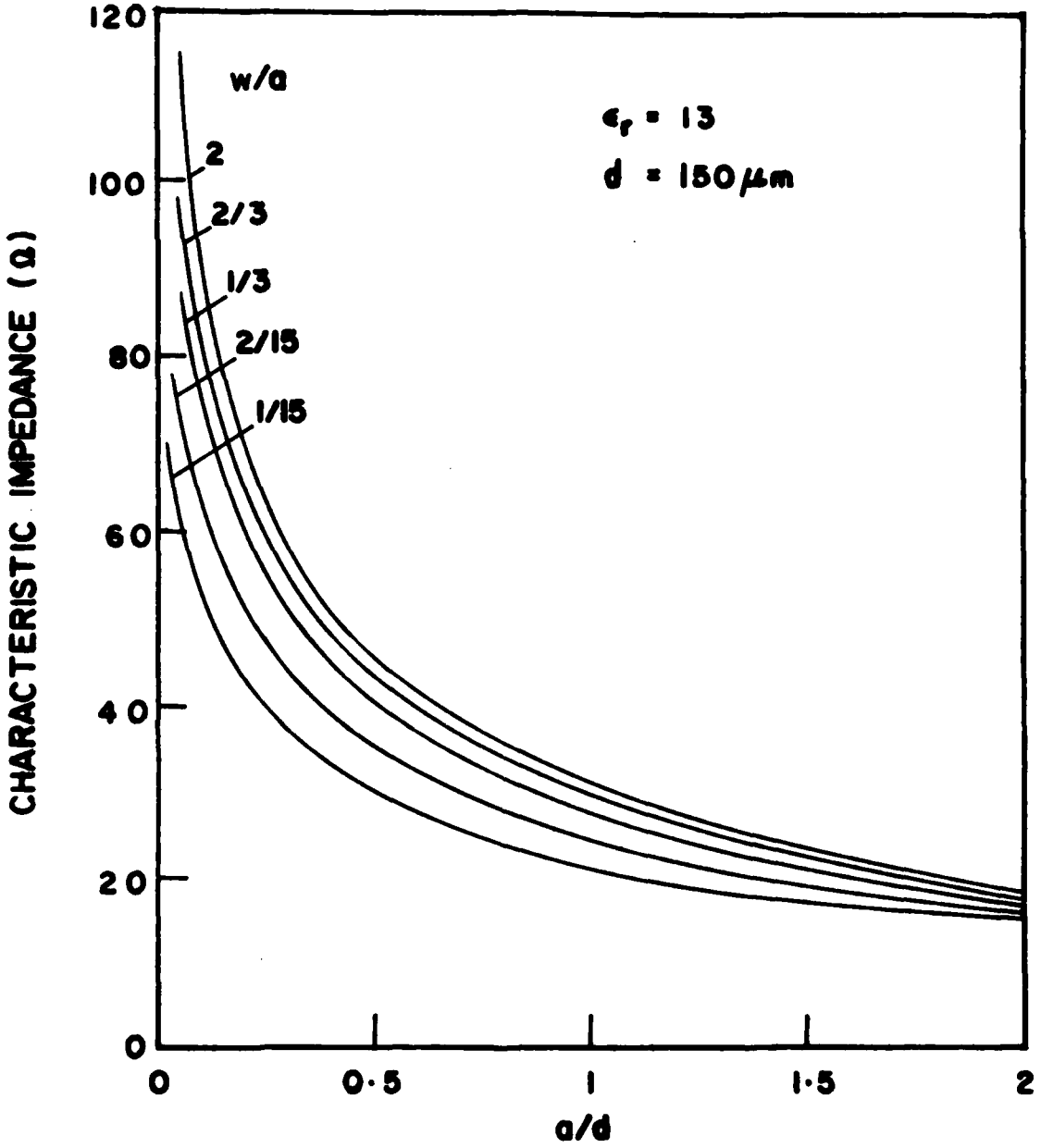

Fig. 10. Characteristic impedance of conductor-backed coplanar waveguide.

as the insulator and Si (ε_r = 12.0) as the semiconductor. They observed that, depending on the frequency and the resistivity of the substrate, three different types of fundamental modes could appear. By their physical behavior, these modes were classified [18,21] into the skin-effect mode, the lossy-dielectric mode, and the slow-wave mode. In particular, the slow-wave mode was found to propagate within the resistivity-frequency range suited to monolithic circuit technology. Extensive experimental results of the propagation constant and characteristic impedance were reported for microstrip lines with narrow and wide strips operating in the slow-wave mode.

The validity of this analysis is verified by Hasegawa's measurements. For the case of a narrow strip (w/d = 0.64), the calculated slow-wave factors and attenuation constants are plotted in Fig. 11 versus frequency. Although only one basis function is used to approximate the strip current, good agreement is found between the analytical and experimental results. The most notable discrepancy in the attenuation constant toward the lower end of frequencies is due to the fact that no conductor loss is considered in the analysis. This is verified by including the conductor losses of the ground plane in the analysis. The results of doing this are presented in Fig. 11 as the dashed lines which show an increase in the attenuation constant at lower frequencies. The conductor losses on the strip have not been considered due to difficulties in the formulation.

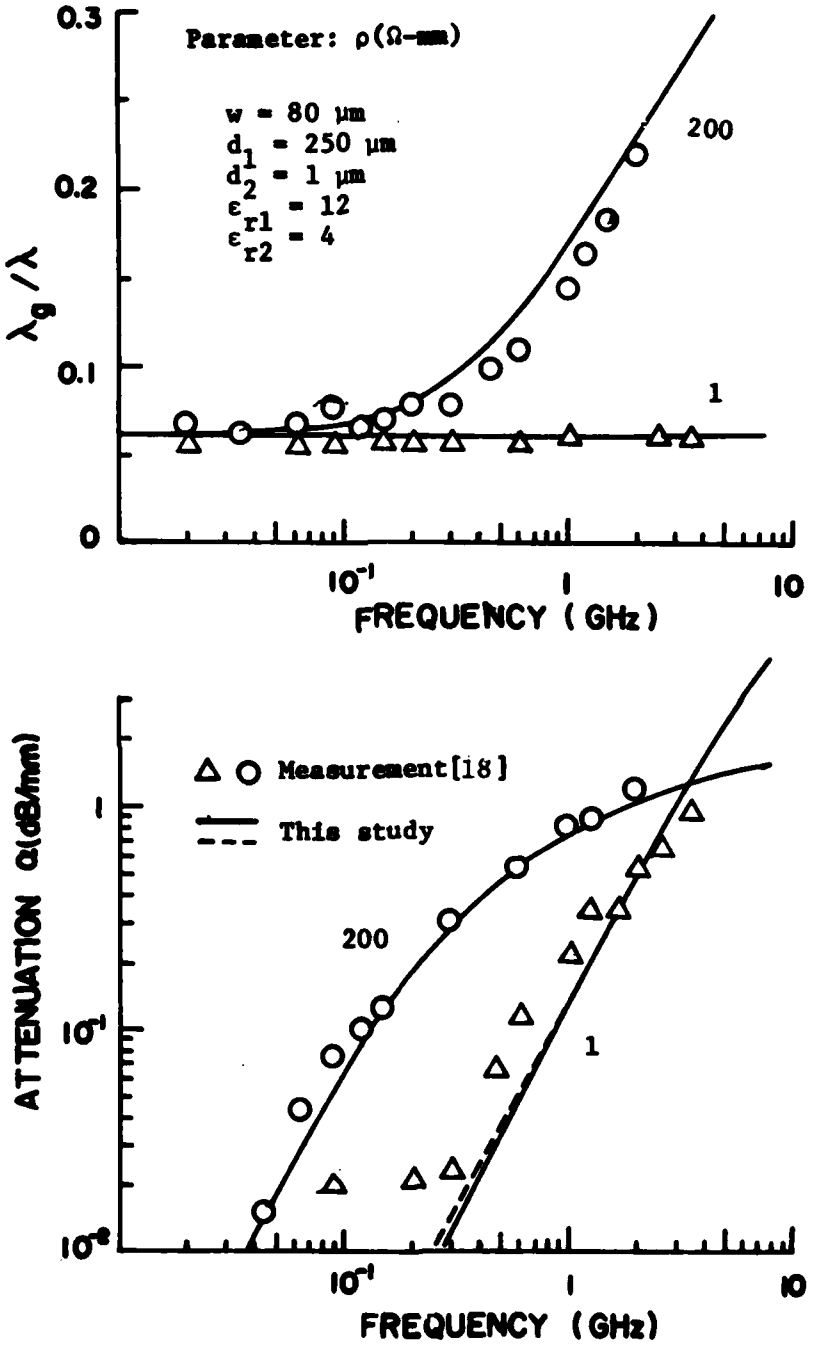

Fig. 11. Disperaion and attenuation characteristics of narrow MIS microstrip lines.

At a fixed frequency of 0.5 GHz the structure is studied by varying the resistivity of the semiconducting substrate. The results are shown in Fig. 12. The optimum resistivity for low-loss propagation is found to be about 1.5 Ω-mm, same as the optimum resistivity predicted using a parallel-plate transmission line model [18].

For a wide strip ($w/d \geq 1$) more basis functions are required to obtain good results. The convergence of the solutions has been tested by increasing the number of basis functions and is tabulated in Table 1. It is found that good results can be obtained by using five basis functions ($M = N = 2$). The slow-wave factors and the attenuation constants shown in Fig. 13 are calculated using these five basis functions. Although the calculations do not show close quantitative agreement with the measurements, they predict correct behavior. The discrepancies are caused in part by neglecting the conductor losses in the system. Another possible source of errors may be due to dimensional uncertainties. For example, if we take the thickness of the insulator (d) as 0.7 μm instead of 1 μm in one of the calculations, the result agrees much better with the measurement as shown in Fig. 13.

The Schottky contact microstrip line tested by Jäger and Rabus [19] was also analyzed. In such structures, the depletion layer is usually localized near the strip. This structure can be approximated by the model in Fig. 8b, because most of the field

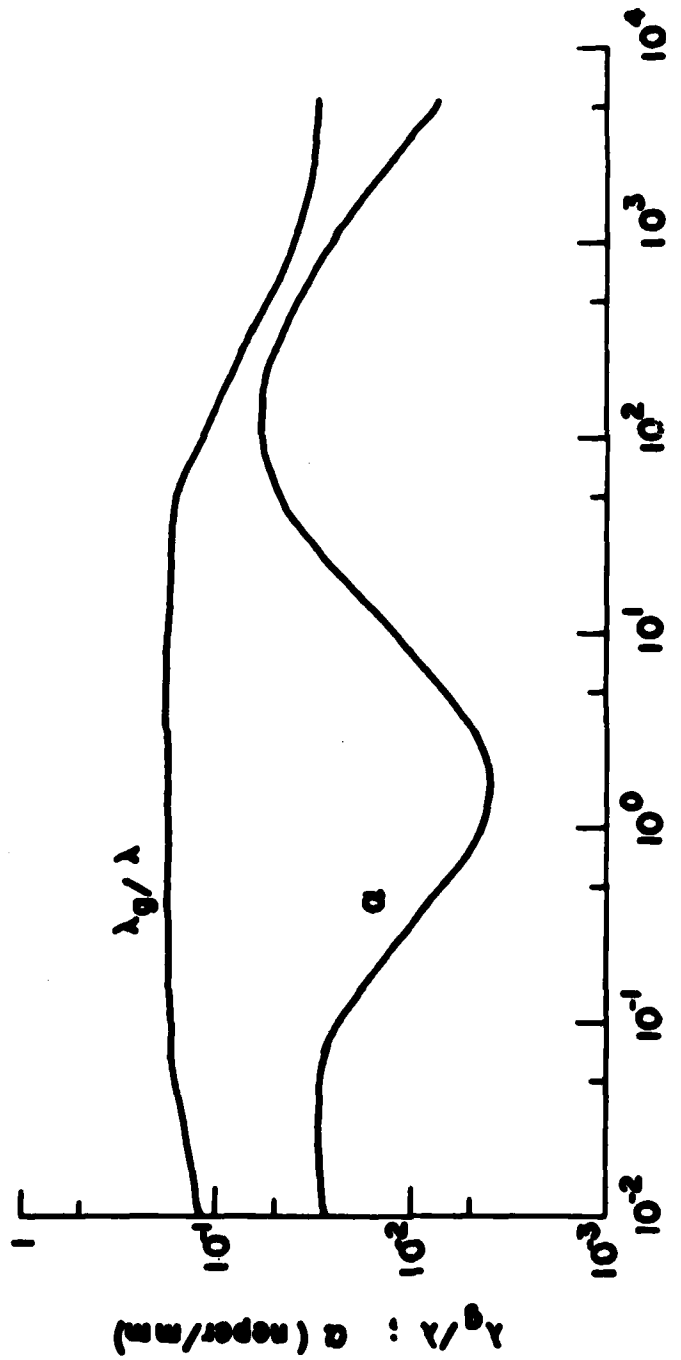

Fig. 12. Slow-wave factor and attenuation of MIS microstrip lines vs. resistivity of semiconductor substrate.

Table 1. Slow-wave factors and attenuation constants of wide MIS microstrip lines.
($w = .254$mm, $b_1 = 1$ μm, $b_2 = .22$ mm)

	f = .1GHz		f = .01GHz	
M = N	λ_g/λ	α(dB/mm)	λ_g/λ	α(dB/mm)
0	.05654	.053308	.054222	.00057301
1	.052178	.074406	.048601	.00084489
2	.051522	.077345	.047834	.00088252
3	.051316	.078228	.047598	.00089380

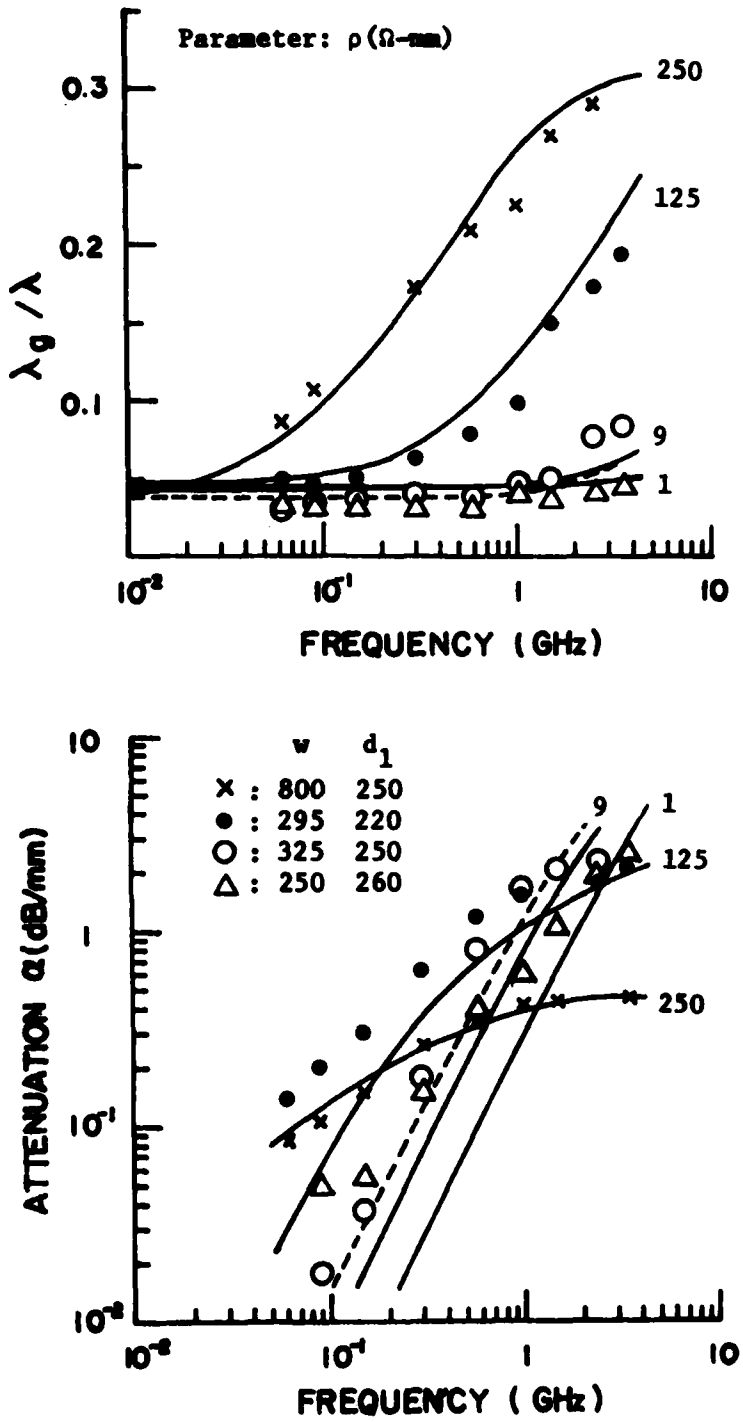

Fig. 13. Dispersion and attenuation of wide MIS microstrip lines.

lines pass through the depletion layer and the field at large distances from the depletion layer has little effect on the propagation characteristics. It should be noted that the frequency-dependent property and fringing-field effect of the structure are correctly incorporated in the present method. Such is not the case in the parallel plate approximation used in [18,19] in which some correction factor must be used. Fig. 14 shows that the present analysis can accurately describe the propagation properties experimentally obtained.

C. MIS Coplanar Waveguides

The MIS coplanar structure in Fig. 8a is also studied with this method and the results are compared with measurements reported in [20,29] in Fig. 15. Good agreement is shown in both the slow-wave factors and attenuation constants. The coplanar line was built on a GaAs substrate with a narrow center strip and wide slots. Since the coupling between slots is strong, a large number of basis functions are required for accurate results. The convergence of solutions has been studied by increasing the number of basis functions used. Typical results are tabulated in Table 2. It is found that good results can be obtained by using seven basis functions that represent axial and transverse electric fields in the slot.

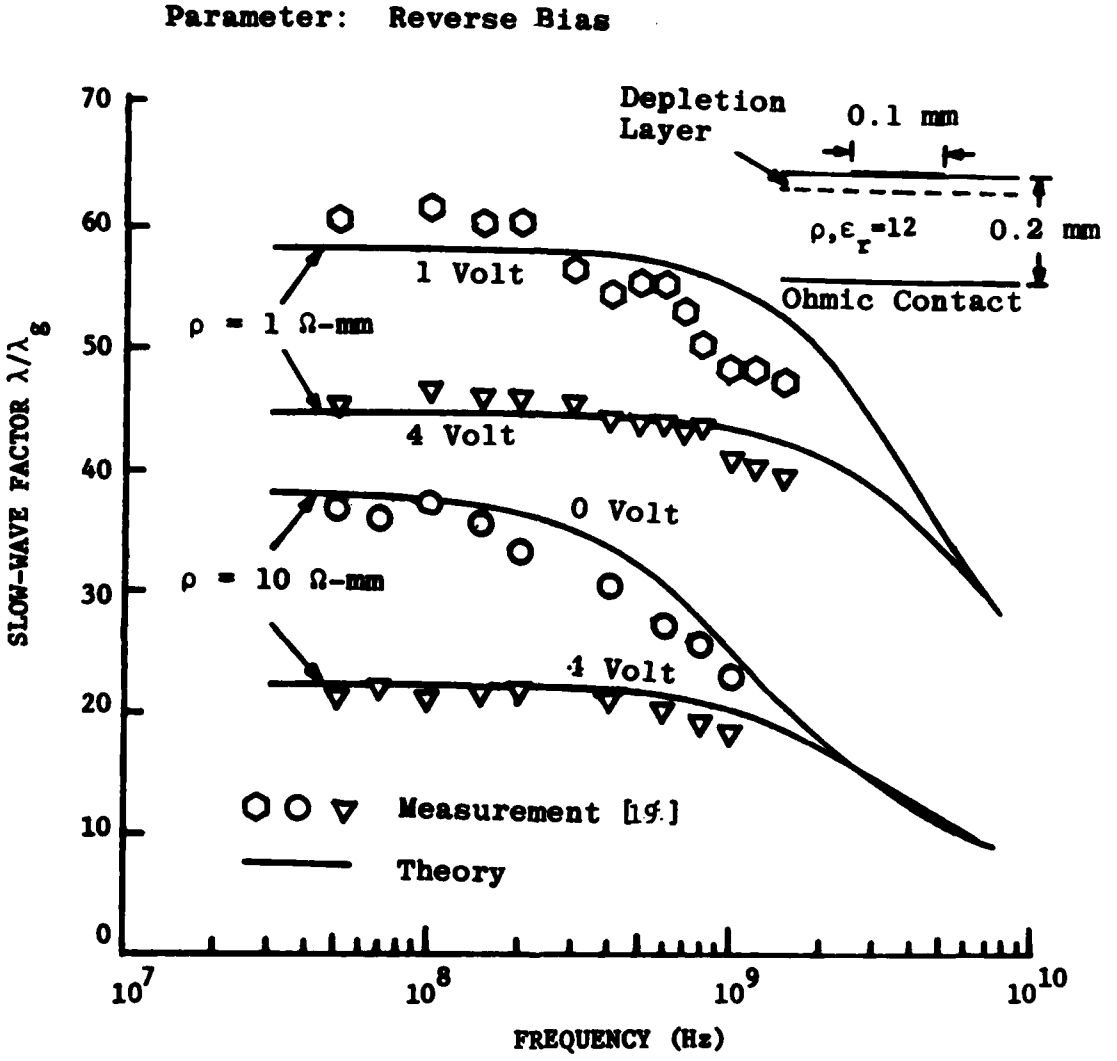

Fig. 14. Slow-wave characteristics of Schottky-barrier microstrip lines.

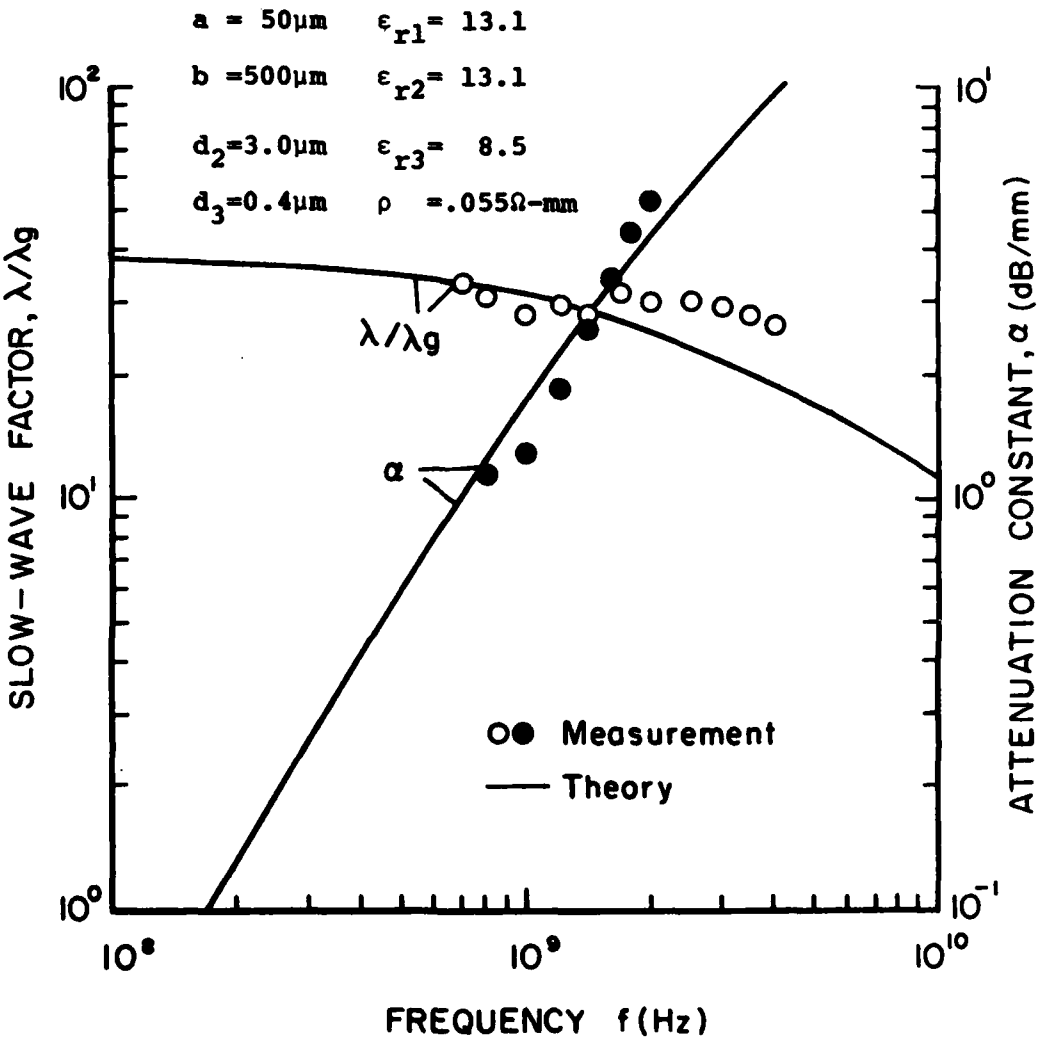

Fig. 15. Dispersion and attenuation of MIS coplanar waveguide.

Table 2. Slow-wave factors and attenuation constants of MIS coplanar waveguide.

	f = 0.1GHz		f = 1.0GHz	
M = N	λ_g/λ	α(dB/mm)	λ_g/λ	α(dB/mm)
0	.019540	.18276	.032517	2.8792
1	.023043	.060137	.030794	2.4416
2	.025519	.049147	.031861	1.9117
3	.026336	.046614	.031633	1.7648

Using the structural parameters given in Fig. 15, a family of curves was generated relating the propagation constant of the MIS coplanar waveguide as a function of frequency to the substrate resistivity. A mode diagram made from these curves is shown in Fig. 16a. The three types of modes found by Hasegawa [18] are clearly shown in this figure. A typical example demonstrating the behavior of the slow-wave factor and attenuation constant at 0.1 GHz with respect to resistivity is given in Fig. 16b and 16c. For this structure the optimum resistivity for low loss propagation is about 1.5×10^{-2} Ω-mm.

A GaAs coplanar structure with Schottky contacted center strip was tested at Hughes Aircraft [30]. The measured slow-wave factors agree reasonably well with those theoretically predicted by the present analysis.

IV. CONCLUSIONS

An efficient numerical method has been proposed to obtain the propagation constant and characteristic impedance of planar transmission lines used in MMICs. This method is based on the application of Galerkin's method in the spectral domain in which the dyadic Green's functions, in the spectral domain, are derived using a simple and fast procedure. This procedure is based on transverse equivalent transmission lines for a spectral wave and on a simple coordinate transformation. Further, a complete set of

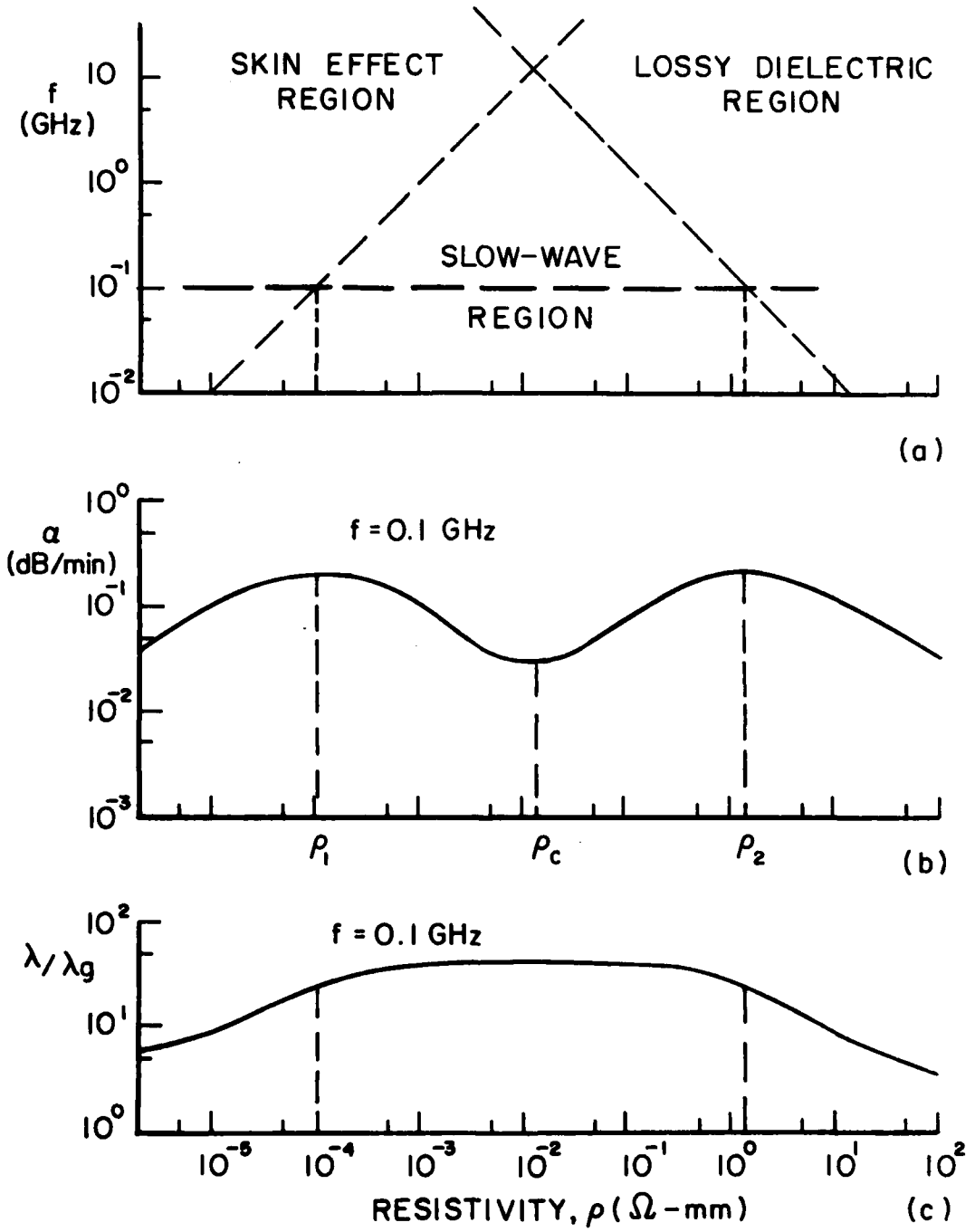

Fig. 16. Characteristics of MIS coplanar waveguide. (a) Mode chart, (b) Attenuation vs. resistivity, (c) Slow-wave factor vs. resistivity.

basis functions is employed so that the convergence of sol
can be tested.

The transmission-line properties of the conductc
coplanar waveguide are analyzed. Since it is a mixture of
strip line and a coplanar waveguide, calculations show tha
erties of each become predominant depending on the structu
meters. For a fixed substrate thickness, the characterist
ance and phase constant may be varied independently by sim
adjusting the widths of the center strip and slots in the
sion line. For a GaAs substrate, the usable practical imp
range is approximately 15-120 Ω.

Microstrip lines and coplanar waveguides formed
and Schottky barrier contacts are also analyzed. The pres
a highly lossy semiconducting substrate is taken into acc
employing a complex permittivity. The final solution is a
propagation constant that is composed of a slow-wave factc
attenuation constant. Depending on the frequency and the
vity of the semiconductor substrate, three different types
damental modes are predicted. The optimum resistivity for
slow-wave propagation can be obtained.

BIBLIOGRAPHY

1. F.J. Moncrief, "Monolithic MICs gain momentum as GasAs MSI nears," Microwaves, Vol. 18, No. 7, pp. 42-53, 1979.

2. H.Q. Tserng, "Advances in microwave GaAs pwoer FET device and circuit technologies, " 11th European Microwave Conference, September 7-10, 1981, pp. 48-58.

3. F.J. Moncrief, "Japan - attention turns to high-power GaAs FETs as low-noise devices reach maturity, "Microwaves, Vol. 19, No. 2, pp. 36-46, 1980.

4. R.S. Pengelly, "Monolithic GaAs ICs tackle analog tasks," Microwaves, Vol. 18, No. 7, pp. 56-65, 1979.

5. R.A. pucel, "Signal and noise properties of GaSa microwave FETs, "Advances in Electronics and Electron Physics, Vol. 38, New York: Academic Press, pp. 195-265, 1975.

6. H.A. Wheeler, "Transmission-line properties of parallel strips separated by a dielectric sheet," IEEE Trans. Microwave Theory Tech., Vol. MTT-13, pp. 172-185, 1965.

7. C.P. Wen, "Coplanar waveguide: A surface strip transmission line, "IEEE Trans. Microwave Theory Tech., Vol. MTT-17, pp. 1087-1900, 1969.

8. H.E. Green, "The numerical solution of some important transmission line problems," IEEE Trans. Microwave Tneory Tech., Vol. MTT-13, pp. 676-692, 1965.

9. P. Daly, "Hybird-mode analysis of microstrip by finite-element method," IEEE Trans. Microwave Theory Tech., Vol. MTT-19, pp. 19-25, 1971.

10. E. J. Denlinger, "A frequency dependent solution of microstrip transmission lines," IEEE Trans. Microwave Theory Tech., Vol. MTT-19, pp. 30-39, 1971.

11. T. Itoh and R. Mittra, "Spectral-domain approach for calculating the dispersion characteristics of microstrip lines," IEEE Trans. Microwave Theory Tech., Vol. MTT-21, pp. 496-499, 1973.

12. T. Itoh and R. Mittra, "Dispersion characteristics of slot lines," Electronics Lett., Vol. 7, No. 13, pp. 364-365, 1971.

13. J. B. Knorr and K. D. Kuchler, "Analysis of coupled slots and coplanar strips on dielectric substrate," IEEE Trans. Microwave Theory Tech., Vol. MTT-23, pp. 541-548, 1975.

14. R. Mittra and T. Itoh, "Charge and potential distributions in shielded striplines," IEEE Trans. Microwave Theory Tech., MTT-18, pp. 149-156, 1970.

15. G. Kowalski and R. Pregla, "Dispersion characteristics of shielded microstrips with finite thickness," Arch. Elektron. Ubertragungstech. Vol. 25, pp. 193-196, 1971.

16. S. B. Cohn, "Slotline on a dielectric substrate," IEEE Trans. Microwave Theory Tech., Vol. MTT-17, pp. 768-778, 1969.

17. R. A. Pucel, "Design considerations for monolithic microwave circuits," IEEE Trans. Microwave Theory Tech., Vol. MTT-29, pp. 513-534, 1981.

18. H. Hasegawa, M. Furukawa and H. Yarai, "Properties of microstrip line on Si-SiO_2 system," IEEE Trans. Microwave Theory Tech., Vol. MTT-19, pp. 869-881, 1971.

19. D. Jager and W. Rabus, "Bias dependent phase delay of Schottky contact microstrip line," Electron. Lett., Vol. 9, No. 9, pp. 201-203, 1973.

20. H. Hasegawa and H. Okizaki, "M.I.S. and Schottky slow-wave coplanar striplines on GaAs Substrates," Electron. Lett., Vol. 13, No. 22, pp. 663-664, 1977.

21. G. W. Hughes and R. M. White, "Microwave properties of nonlinear MIS and Schottky-Barrier microstrip," IEEE Trans. Electron Dev., Vol. ED-22, pp. 945-956, 1975.

22. J.M. Jaffe, "A high-frequency variable delay line," IEEE Trans. Electron Dev., Vol. ED-19, pp. 1292 - 1294, 1972.

23. R.H. Jansen, "High-speed computation of single and coupled microstrip parameters including dispersion, high-order modes, loss and finite strip thickness,"IEEE Trans. Microwave Theory Tech., Vol. MTT-26, pp. 75-82, 1978.

24. T. Itoh, "Spectral domain immittance approach for dispersion characteristics of generalized printed transmission lines," IEEE Trans. Microwave Theory Tech., Vol. MTT-28, pp. 733-736, 1980.

25. G.I. Zysman and D. Varon, "Wave propagation in microstrip transmission lines," Intl. IEEE-MTT Symp., Dallas, TX, May 1969, pp. 3-9.

26. R.F. Harrington, Time-Harmonic Electromagnetic Fields (New York: McGraw-Hill, 1961).

27. R. Mittra and S.W. Lee, Analytical Techniques in the Theory of Guided Waves (New York: Macmillan, 1971), pp. 4-11.

28. L.P. Schmidt and T. Itoh, "Spectral domain analysis of dominant and higher order modes in fin-lines,"IEEE Trans. Microwave Theory Tech., Vol. MTT-28, pp. 981-985, 1980.

29. S. Seki and H. Hasegawa, "Cross-tie slow-wave coplanar waveguide on semi-insulating GaAs substrate," Electron. Lett., vol, 17, No. 25, pp. 940-941, 1981.

30 J. Schellenberg, Private communication.

END

FILMED

7-84

DTIC